ACS Catalysis

Research Article

Cite This: ACS Catal. 2019, 9, 4764–4776

pubs.acs.org/acscatalysis

Biocatalytic Carbon–Hydrogen and Carbon–Fluorine Bond Cleavage through Hydroxylation Promoted by a Histidyl-Ligated Heme Enzyme

Yifan Wang,[†] Ian Davis,[†] Inchul Shin,[†] Daniel J. Wherritt,[†] Wendell P. Griffith,[†] Kednerlin Dornevil,[†] Keri L. Colabroy,[‡] and Aimin Liu*[,†]

[†]Department of Chemistry, University of Texas, San Antonio, Texas 78249, United States

[‡]Department of Chemistry, Muhlenberg College, Allentown, Pennsylvania 18104, United States

Supporting Information

ABSTRACT: LmbB2 is a peroxygenase-like enzyme that hydroxylates L-tyrosine to L-3,4-dihydroxyphenylalanine (DOPA) in the presence of hydrogen peroxide. However, its heme cofactor is ligated by a proximal histidine, not cysteine. We show that LmbB2 can oxidize L-tyrosine analogues with ring-deactivated substituents such as 3-nitro-, 3-fluoro-, 3-chloro-, and 3-iodo-L-tyrosine. We also found that the 4-hydroxyl group of the substrate is essential for reacting with the heme-based oxidant and activating the aromatic C–H bond. The most interesting observation of this study was obtained with 3-fluoro-L-tyrosine as a substrate and mechanistic probe. The LmbB2-mediated catalytic reaction yielded two hydroxylated products with comparable populations: i.e., oxidative C–H bond cleavage at C5 to generate 3-fluoro-5-hydroxyl-L-tyrosine and oxygenation at C3 concomitant with a carbon–fluorine bond cleavage to yield DOPA and fluoride. An iron protein mediated hydroxylation on both C–H and C–F bonds with multiple turnovers is unprecedented. Thus, this finding reveals a significant potential of biocatalysis in C–H/C–X bond (X = halogen) cleavage. Further ^{18}O-labeling results suggest that the source of oxygen for hydroxylation is a peroxide and that a commonly expected oxidation by a high-valent iron intermediate followed by hydrolysis is not supported for the C–F bond cleavage. Instead, the C–F bond cleavage is proposed to be initiated by a nucleophilic aromatic substitution mediated by the iron hydroperoxo species. On the basis of the experimental results, two mechanisms are proposed to explain how LmbB2 hydroxylates the substrate and cleaves C–H/C–F bonds. This study broadens the understanding of heme enzyme catalysis and sheds light on enzymatic applications in medicinal and environmental fields.

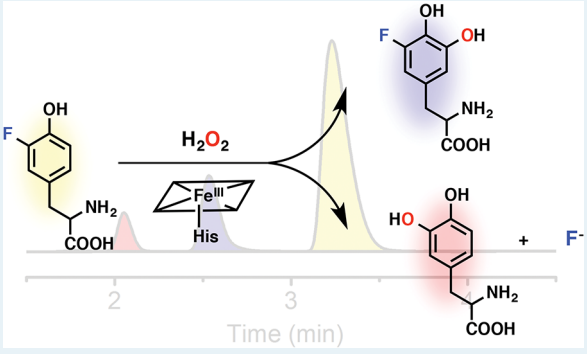

KEYWORDS: *heme chemistry, C–H/C–F bond cleavage, dehalogenation, DOPA, histidyl-ligated heme, tyrosine hydroxylase*

INTRODUCTION

The enzymatic hydroxylation of an aromatic ring is a chemical reaction with vast history and utility. Enzymatic aromatic ring hydroxylation is an essential step in the activation and degradation of molecules by the human liver and of natural and unnatural aromatic molecules by microorganisms in groundwater and soil.[1,2] It is known that aromatic rings are hydroxylated by NADH-dependent P450s,[3] pterin- or α-ketoglutarate-dependent nonheme iron monooxygenases,[4] diiron hydroxylases,[5] type III copper-mediated monooxygenases,[6] and flavin-dependent monooxygenases[7] with either molecular oxygen or hydrogen peroxide as their oxidants. Recently, reports of a new type of enzymatic hydroxylase activity on L-tyrosine have surfaced from the gene clusters of natural product biosynthesis.[8] The first of these L-tyrosine hydroxylases was identified as LmbB2 from the biosynthetic gene cluster of the antibiotic lincomycin;[9] additional homologues were later identified in hormaomycin[10] and four pyrrolo[1,4]benzodiazepine gene clusters of anthramycin,[11] sibiromycin,[12] tomaymycin,[13] and poranthramycin.[14] These clinically important natural products contain a structurally similar pyrroline moiety (Scheme 1A). The biosynthesis of such a pyrroline moiety starts with L-tyrosine hydroxylation to L-3,4-dihydroxyphenylalanine (DOPA) by these LmbB2-like L-tyrosine hydroxylases (Scheme 1B).[10,15,16] Preliminary biochemical studies on representative examples of these hydroxylases indicate that the hydroxylation was accomplished with a histidyl-ligated heme cofactor.[11,17] A heme ligated by histidine in the axial position distinguishes the LmbB2-like enzymes from other hemoproteins with established biological roles as hydroxylases. The cytochrome P450 enzymes and peroxygenases bind heme with axial cysteine-based thiol

Received: January 18, 2019
Revised: April 5, 2019
Published: April 11, 2019

DOI: 10.1021/acscatal.9b00231
ACS Catal. 2019, 9, 4764–4776

Scheme 1. (A) Natural Antibiotics, Including Lincomycin, Sharing a Similar Pyrroline Moiety (Highlighted in Purple) and (B) a New Class of L-Tyrosine Hydroxylases (Highlighted in Navy) Involved in the First Step of the Pyrroline Moiety Biosynthesis, Which Converts L-Tyrosine to DOPA in the Presence of Hydrogen Peroxide

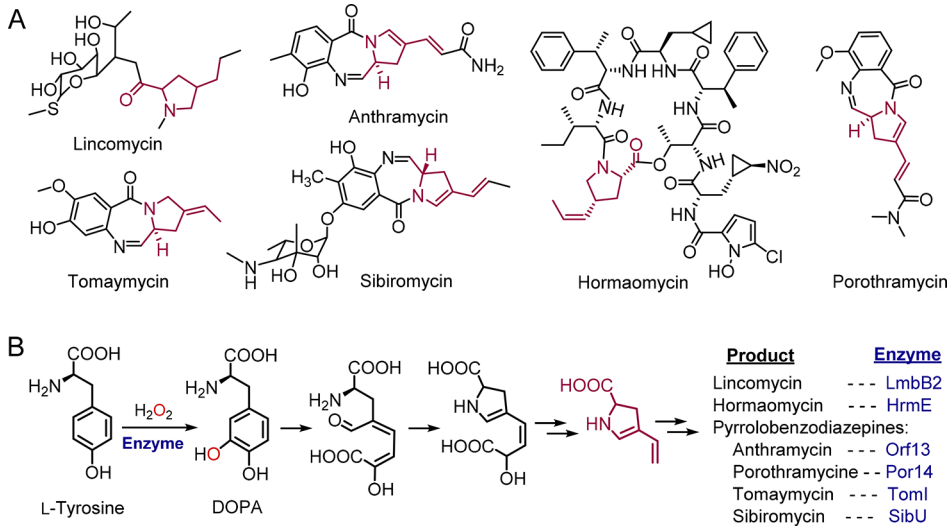

Scheme 2. Summary of the LmbB2 Reaction for (A) L-Tyrosine (1, and Product 1a), (C) 3-Nitro-L-Tyrosine (4, and Product 4a), and (D) 3-Fluoro-, 3-Chloro-, and 3-Iodo-L-Tyrosine (5−7 and Products 5a−7a, Respectively) and (B) L-Phenylalanine (2) and *O*-Methyl-L-Tyrosine (3) Failure To Yield Detectable Reaction Product

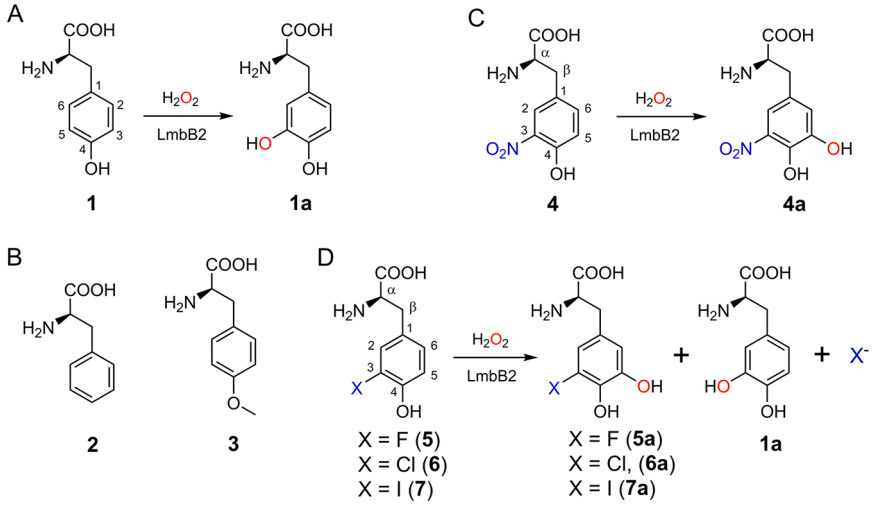

ligands, and it has been persuasively argued from a variety of experimental data that the identity and H-bonding environment of the axial ligand directly affect the redox potential of the heme and its ability to perform C−H bond activation and oxygen atom transfer.[18−21] Therefore, understanding the mechanism of L-tyrosine hydroxylases is not a simple extrapolation from previous work on aromatic hydroxylation systems, and careful study of the reaction chemistry and mechanism is warranted.

In this study, our exploration of the enzymatic mechanism for tyrosine hydroxylase with unnatural substrate analogues and biophysical methods has revealed an unprecedented enzyme-catalyzed carbon−halogen (C−X) bond cleavage mechanism from halogenated L-tyrosine derivatives. EPR and HPLC results suggested that the histidyl-ligated enzyme can oxidize a range of tyrosine analogues even with strong ring-deactivating substituents. The product analyses demonstrated that LmbB2 can activate either C−H or C−X bonds, resulting in the departure of a proton or halide anion. Quantitative analyses indicated the C−H and C−X bond cleavage are from two independent reactions with multiple turnovers, and the highest yield of C−X cleavage was observed for fluorinated tyrosine. Analyzing isotope distribution on products with ^{18}O-enriched peroxide or water suggests that the aromatic hydroxylation is driven by peroxide derivatives instead of water. Together, mechanistic pathways for C−H and C−X bond cleavage are proposed and discussed, and a biocatalytic C−H and C−F bond hydroxylation promoted by a histidyl-ligated heme enzyme is reported for the first time. Our characterization of this powerful chemistry from a naturally occurring heme oxidant not only broadens our overall understanding of heme enzyme catalysis but also raises important implications for the pharmaceutical design of aryl−halogen-containing drugs and bioremediation of environmental contaminants.

DOI: 10.1021/acscatal.9b00231
ACS Catal. 2019, 9, 4764−4776

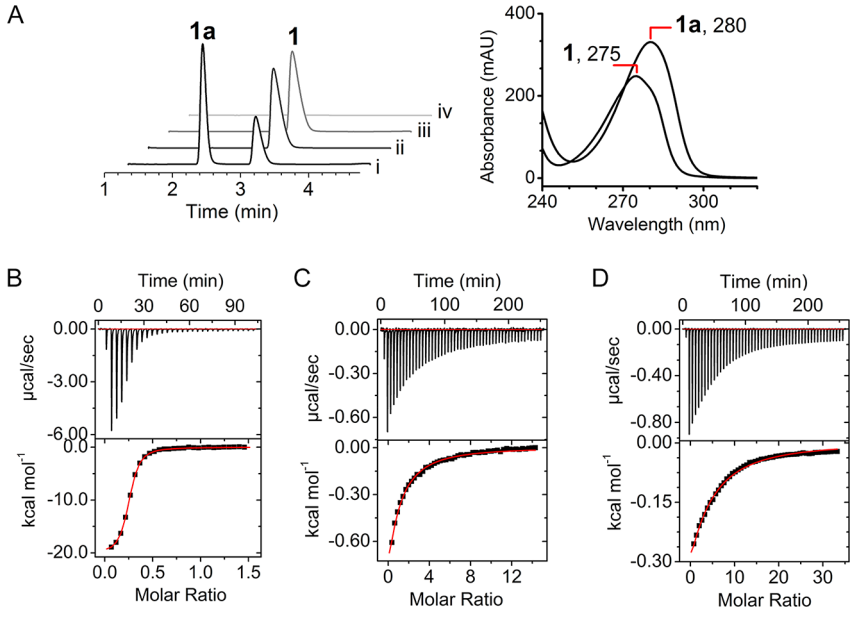

Figure 1. HPLC profile of the LmbB2 reaction showing L-tyrosine (**1**) hydroxylation to DOPA (**1a**) and the UV−vis spectra (A): (i) 100 μM enzyme, 3 mM L-tyrosine and 3 mM H_2O_2 and three controls with (ii) 100 μM enzyme and 3 mM L-tyrosine, (iii) 3 mM L-tyrosine and 3 mM H_2O_2, and (iv) 100 μM enzyme and 3 mM H_2O_2. ITC binding assays showing LmbB2 binding to **1** (B), **2** (C) and **3** (D) with K_D values of 1.35 ± 0.03, 318 ± 8, and 1294 ± 141 μM, respectively.

RESULTS

LmbB2 Requirement of 4-Hydroxyl of Phenolic Amino Acids for Action. The tyrosine hydroxylase from *Streptomyces lincolnensis* (*Sl*TyrH), LmbB2, was purified as described in Materials and Methods and assayed for hydroxylation activity. The isolated enzyme was able to hydroxylate L-tyrosine (**1**) using H_2O_2 as the oxidant, producing DOPA (**1a**) (Scheme 2A), as shown by HPLC at room temperature (Figure 1A), under conditions similar to those previously reported for the homologue Orf13.[11] In order to investigate the potential range of substrates, several substrate analogues were assayed. We first tested the requirement of a hydroxyl group at the 4-position during LmbB2-mediated hydroxylation by assaying L-phenylalanine (**2**) and *O*-methyl-L-tyrosine (**3**) as possible substrates. The former (**2**) does not contain a hydroxyl group, and the hydroxyl group of the latter (**3**) is protected in the form of a methoxy moiety (Scheme 2B). Initial observations from the assays indicated **2** and **3** were not substrates of the enzyme, as we did not detect any measurable reaction product from either analogue regardless of concentration (up to 20 mM), pH (7−10), or oxygen source: i.e., H_2O_2 and peracetic acid (PAA) (Figure S1A,B). These results suggest an essential role for the 4-hydroxyl group during catalysis.

However, before a firm conclusion can be drawn regarding the catalytic role of the hydroxyl group, it is necessary to exclude the possibility that the nonreactive nature of these analogues is simply due to a binding problem. Therefore, binding of **1**−**3** to LmbB2 was assessed by isothermal titration calorimetry (ITC), and the results revealed K_D values of 1.35 ± 0.03, 318 ± 8, and 1290 ± 140 μM, respectively (Figure 1B). Binding constants for analogues **2** and **3** imply substantially lower affinity in comparison to the native substrate; however, these K_D values are well below the actual substrate concentration used in the activity assay experiments, which guarantees sufficient binding of **2** and **3** under the conditions of the reaction.

To further probe whether **2** and **3** bind to the enzyme active site in a manner analogous to that for **1**, we performed an electron paramagnetic resonance (EPR) analysis of the electronic structure of the ES complex. The EPR data collected on the enzyme bound to substrate **1** and analogues **2** and **3** further support the above interpretation. The LmbB2 protein was anaerobically reduced to the ferrous state and then exposed to an excess of nitric oxide (•NO) to form a reduced enzyme-nitrosyl (E-NO•) complex. The E-NO• complex was then mixed with **1**, **2**, or **3** anaerobically in parallel experiments and frozen in liquid nitrogen before measurement by EPR spectroscopy. The EPR spectrum for an E-NO• complex in the absence of any other exogenous ligand exhibited a rhombic signal with an average g value (g_{ave}) of 2.030 and some hyperfine splitting from •NO (Figure 2A). This spectrum represents a typical low-spin six-coordinated S = 1/2 histidine-ligated Fe(II) heme-NO• complex, which has been observed in

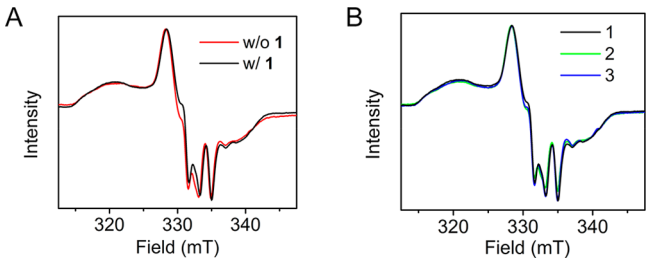

Figure 2. (A) EPR spectra of ferrous enzyme-NO• (E-NO•) complex alone and in a mixture with **1**. In the absence of **1**, E-NO• had a rhombic signal with hyperfine splitting from •NO, with g_{ave} = 2.030; after binding with **1**, the g_{ave} value slightly shifted. (B) Spectra of E-NO• binding with **1**−**3**. The g_{ave} values were 2.027, 2.027, and 2.026, respectively. All spectra were obtained at 50 K, 9.6 GHz microwave frequency, and 0.05 mW power.

DOI: 10.1021/acscatal.9b00231
ACS Catal. 2019, 9, 4764−4776

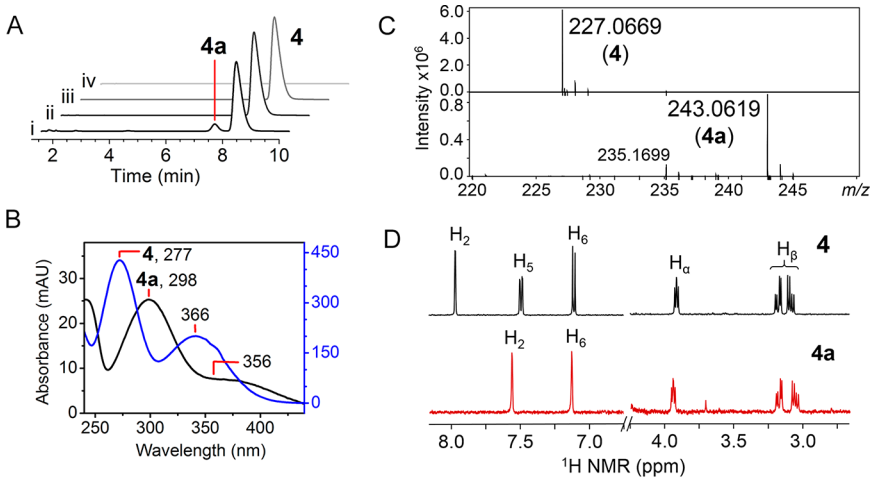

Figure 3. LmbB2 reaction with 3-nitro-L-tyrosine (**4**) generating 3-nitro-5-hydroxyl-L-tyrosine (**4a**). (A) A small product peak was detected by HPLC. The setup for the catalytic reaction was the enzyme with **4** and H_2O_2 (i). Three controls were done with (ii) the enzyme and **4**, (iii) **4** and H_2O_2, and (iv) the enzyme and H_2O_2. (B) Absorbance spectra of **4** (blue) and **4a** (black). (C) High-resolution mass spectra of **4** and **4a**. (D) ^{1}H NMR analysis of **4** and **4a**. Hydrogen atoms are labeled according to the numbering of carbon.

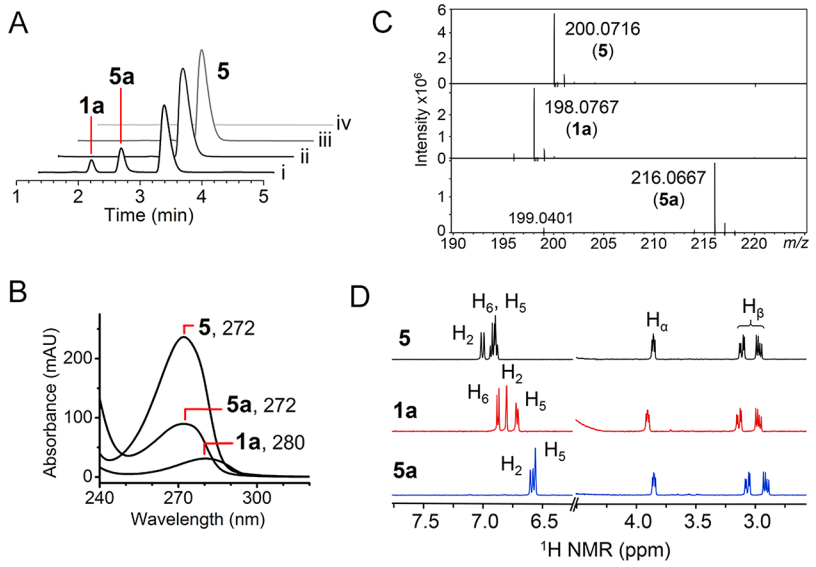

Figure 4. Two products, DOPA (**1a**) and 3-fluoro-5-hydroxyl-L-tyrosine (**5a**), detected by HPLC when LmbB2 reacted with 3-fluoro-L-tyrosine (**5**). (A) HPLC profile. The setup for the enzymatic reaction was (i) LmbB2 with **5** and H_2O_2. Three controls were conducted with (ii) LmbB2 and **5**, (iii) **5** and H_2O_2, and (iv) LmbB2 and H_2O_2. (B) Absorbance spectra of **5**, **1a**, and **5a**. (C) High-resolution mass spectra of **5**, **1a**, and **5a**. (D) ^{1}H NMR analysis for **5**, **1a**, and **5a**. Hydrogen atoms are labeled according to the numbering of carbon.

other biological systems.[22,23] In the presence of 20 mM of **1**, the EPR spectrum shifted upfield. Such a small change indicates that **1** binds to a site adjacent to the heme iron. A direct ligation of **1** to the Fe would have a much larger effect on the spectrum. The E-NO$^\bullet$ EPR signal is very sensitive to a change at the active site, and therefore, even very small changes in the signal reflect alterations in electronic properties of the iron center. The anaerobic addition of 20 mM **2** or **3** to the E-NO$^\bullet$ complex produced EPR spectra similar to that of **1** with an upfield shift (Figure 2B). The g_{ave} values after addition of **1**, **2**, or **3** were 2.027, 2.027, and 2.026, respectively. The nearly identical g_{ave} values and spectral changes suggest a similar microenvironment of ES-NO$^\bullet$ after binding of those ligands, which all differ from the E-NO$^\bullet$ signal alone. *N*-boc-L-tyrosine and *p*-cresol were selected as negative controls of the EPR experiments. The former has a bulky modification on its amino group, and the latter lacks an amino acid moiety; hence, they should not show strong binding to the active site of LmbB2. The LmbB2 E-NO$^\bullet$ complex in the presence of either compound had no significant EPR spectroscopic change in comparison with E-NO$^\bullet$ alone and the same g_{ave} values (Figure S2). These EPR data support the assertion that **2** and **3** bind to the active site in a manner consistent with the natural substrate **1**.

Reaction of LmbB2 and L-Tyrosine Analogues with Electron-Deficient Substitutions. We selected analogues with strong electron-withdrawing groups of nitro and three halide substitutions with increasing atom size and decreasing electronegativity. When 3-nitro-L-tyrosine (**4**) was used as a substrate of LmbB2, a small product peak was observed in the HPLC elution profile (Figure 3A) with absorption λ_{max} at 298 nm and a broad absorbance band around 356 nm (Figure 3B). High-resolution mass spectrometry (HRMS) analysis showed an *m*/*z* value of 243.0619 (Figure 3C), corresponding to 3-

DOI: 10.1021/acscatal.9b00231
ACS Catal. 2019, 9, 4764−4776

nitro-5-hydroxyl-L-tyrosine (**4a**, theoretical *m*/*z* 243.0612 Da, mass accuracy 2.88 ppm). ^{1}H NMR analysis further identified the product as **4a** (Figure 3D). **4** had resonances at 7.97, 7.50, and 7.11 ppm arising from the aromatic hydrogens on C2, C5, and C6, respectively. The aromatic hydrogens of the eluted product were on C2 and C6 at 7.75 and 7.13 ppm, which confirmed that C5 was hydroxylated, generating **4a**. Hydrogens on C_α and C_β had chemical shifts at around 3.9 and 3.1 ppm. These results established a reaction scheme shown in Scheme 2C. These data are consistent with previous reports and our data, which assert that LmbB2 hydroxylation is specific to the C3 or C5 position of L-tyrosine, yielding DOPA as the only product.[11,17] The inefficient conversion of **4** to **4a** is likely due to the ineffective binding caused by the bulky nitro group and the deactivation of the phenyl ring by the nitro substituent. Nevertheless, any production of **4a** from such a heavily deactivated tyrosine ring implies that the LmbB2 heme-based oxidant is highly potent.

Next, we tested LmbB2 reactivity toward three halogenated tyrosine analogues, 3-fluoro-L-tyrosine (**5**), 3-chloro-L-tyrosine (**6**), and 3-iodo-L-tyrosine (**7**). Surprisingly, each of the compounds yielded two products in HPLC assays. The binding affinities for the aforementioned analogues were assessed by ITC (Figure S3). The results showed that **5** has the highest binding affinity among four reactive analogues with a K_D value of 22.2 ± 1.1 μM, around 16-fold weaker than that of the native substrate. The K_D values of **6** and **7** exponentially increase with the size of the halogen atom, at 346 ± 2 and 7820 ± 180 μM, respectively. The bulky nitro substitution of **4** resulted in no detectable thermal change by an ITC experiment, even though some activity was observed. All of the thermodynamic data from ITC are summarized in Table S1.

In the case of the LmbB2 reaction with **5** (Figure 4A), the first eluted product had a retention time and absorption (2.2 min, 280 nm) consistent with **1a**, while the second eluted product had an absorption maximum at 272 nm (Figure 4B). On the basis of the extinction coefficient and HPLC peak integration,[24−26] comparable amounts of products were produced with an estimated ratio of 2/1. Subsequent HRMS suggested that the first product lost a fluorine atom but gained a hydroxyl group as **1a** (measured *m*/*z* 198.0767 Da, theoretical *m*/*z* 198.0761 Da, mass accuracy 3.03 ppm), while the second product had only one additional oxygen atom (measured *m*/*z* 216.0667 Da, theoretical *m*/*z* 216.0667 Da, mass accuracy <0.5 ppm) corresponding to 3-fluoro-5-hydroxyl-L-tyrosine (**5a**) (Figure 4C). Our ^{1}H NMR analysis confirmed the structure assignments (Figure 4D): the substrate **5** had a doublet at 7.00 ppm from the hydrogen at C2, a multiplet around 6.96−6.86 ppm from the two hydrogens on C5 and C6, the first eluted product corresponds to **1a**, which had resonances at 6.87, 6.80, and 6.71 ppm arising from hydrogens on C5, C2, and C6, respectively, and the later eluted product corresponds to **5a**, which had resonances at 6.59 and 6.56 ppm from hydrogens on C2 and C6, respectively. The resonances at around 3.9 and 3.0 ppm corresponding to hydrogens on C_α and C_β had no significant chemical shift changes.

To determine if LmbB2 would hydroxylate at both C3 and C5 for other C3-halogenated substrates, reactions using **6** and **7** as alternate substrates were conducted. The results obtained further elaborated the observation with **5**. Indeed, LmbB2 catalyzes the expected hydroxylation at C5 and also the surprising hydroxylation at C3 requires apparent breakage of the carbon−halogen (C−X) bond to produce **1a**. Examination of the LmbB2 reaction with **6** revealed product **6a** predominantly; only a small fraction was transformed into **1a** (Figure S4). In the assay of **7**, less substrate was hydroxylated. Most was converted to **7a**, while **1a** was present in trace amounts (Figure S5). Therefore, a reaction scheme for three halogen-substituted analogues is summarized in Scheme 2D. The ratio of **1a** formation among the reactions of substrates **5**−**7** was 4.5/1.3/1 after normalizing for the percentage of substrate conversion (Table S2). Although **5** produced the most **1a**, in both absolute and relative terms, **6** showed the most overall activity among the analogues tested, which may result from its relatively tight binding and weaker ring deactivation. Overall, more **1a** was formed in the reaction of **5** in comparison to **6** and **7** presumably because fluorine has the smallest steric effect among the halogens. Even though the C−F bond has the strongest strength and thermal stability among the three carbon−halogen bonds, its cleavage is more effective than for other carbon−halogen bonds.

Mechanistic Investigation of C−H versus C−F Bond Cleavage by LmbB2. The formation of **5a** is predictable as a result of an anticipated hydroxylation, because the normal hydroxylation takes place on the only possible vacant site: i.e., C5 for **5**. However, the formation of **1a** is an entirely unexpected outcome, since it would require carbon−fluorine (C−F) bond cleavage. To verify the predicted loss of fluorine, ^{19}F NMR analysis was conducted on the LmbB2 reaction of **5** with different amounts of H_2O_2 (Figure 5A). The starting reaction mixture of LmbB2 and **5** without peroxide gave only a doublet of doublets at −137.68 ppm expected for **5**. After

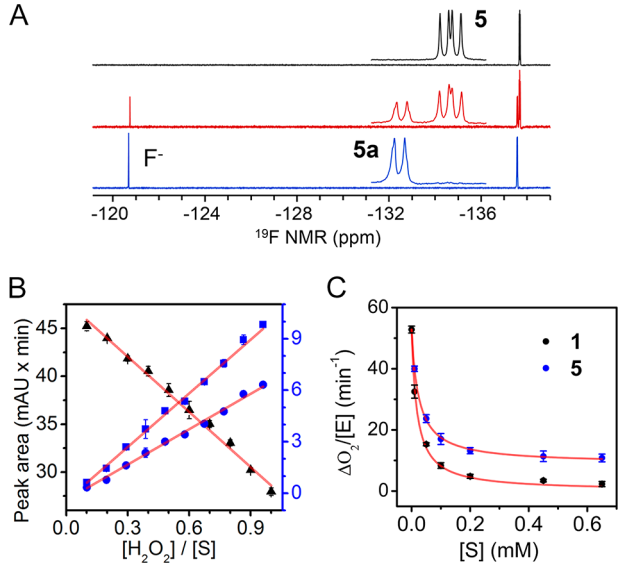

Figure 5. (A) ^{19}F NMR spectra of in-tube reactions: (black) 3-fluorotyrosine (**5**) and LmbB2; (red) partial conversion of **5** to 3-fluoro-5-hydroxyl-L-tyrosine (**5a**) and fluoride with addition of 0.5 equiv of H_2O_2; (blue) almost complete conversion of **5** to **5a** and fluoride with addition of 1.5 equiv of H_2O_2. The insets show the enlarged spectra for **5** and **5a**. (B) HPLC analysis. The decay of **5** (black triangles) and the formation of DOPA (**1a**, blue circles) and **5a** (blue squares) had a linear relation to H_2O_2 concentration. (C) Oxygen production rate as a function of the concentration of L-tyrosine (**1**) and **5** in the presence of 1 mM H_2O_2. The fitting method is described in the Supporting Information.

DOI: 10.1021/acscatal.9b00231
ACS Catal. 2019, 9, 4764−4776

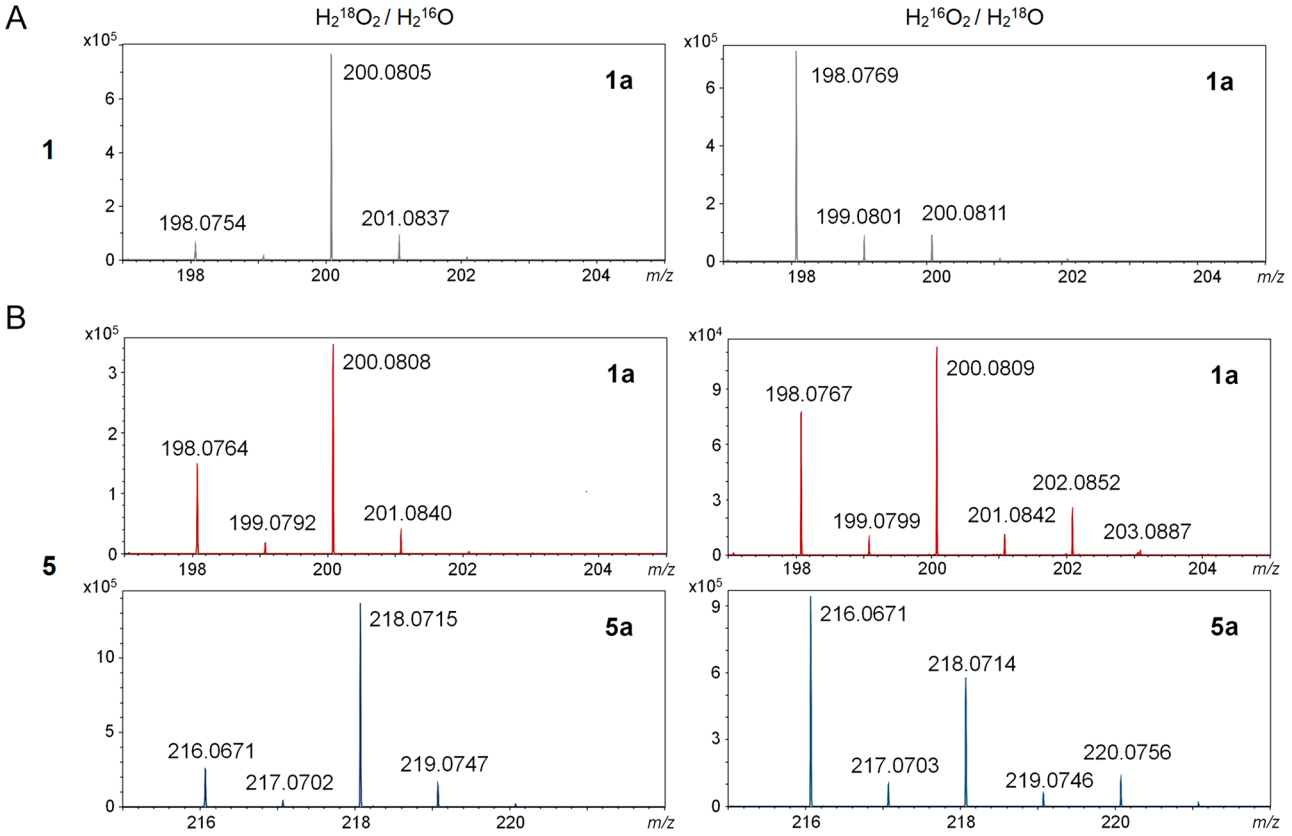

Figure 6. High-resolution mass spectrometry analyses of the isotope labeling reaction using ^{18}O-enriched H_2O_2 (left panels) or H_2O (right panels). Only DOPA (**1a**) was produced when L-tyrosine was used as a substrate (A), while both **1a** and 3-fluoro-5-hydroxyltyrosine (**5a**) (B) were observed using 3-fluoro-L-tyrosine as substrate. **1a** and **5a** have molecular weights of 198.0761 and 216.0667 Da with natural abundance.

addition of 0.5 equiv of H_2O_2, the peak corresponding to **5** decreased while an adjacent doublet at −137.58 ppm and a singlet at −120.74 ppm were generated, corresponding to **5a** and fluoride, respectively. With 1.5 equiv of H_2O_2, the signal for **5** was completely converted to **5a** and F^-. These data are consistent with robust oxidation of **5** by LmbB2 at both C3 and C5. LmbB2 is able to hydroxylate at C5 to produce **5a** and also at C3, cleaving the aromatic C−F bond and generating **1a** with loss of the fluorine atom as a fluoride anion. It is noticeable that at least 1.5 equiv of H_2O_2 was required to perform the complete conversion. Taken together, the HPLC, MS, and NMR evidence of **5a**, **1a**, and F^- demonstrate the strong capacity for enzyme hydroxylation at C3 or C5 positions, despite the difficulty of C−F bond cleavage. Moreover, the continuous formation of **1a** and F^- is evidence that the heme catalytic center returns to the resting state after each turnover of substrate-based C−F bond hydroxylation and that the creation of **1a** and F^- is the result of enzymatic catalysis.

The evidence of C3 hydroxylation with the C−F bond cleavage and formation of **1a** as well as C5 hydroxylation and formation of **5a** prompted further investigation into the mechanism. To investigate whether the formation of C3 and C5 hydroxylation products is a processive versus an independent process, the enzymatic reaction of **5** was examined with increasing concentrations of peroxide and analyzed by HPLC. It should be noted that the peroxide addition for each targeted concentration was not made at once but with multiple additions at a smaller quantity to avoid undesired protein damage which occurs at high peroxide concentrations. Plotting the integrated peak area of **5**, **5a**, and **1a** as a function of the H_2O_2 concentration revealed that substrate decay and the two product formations were linearly dependent on H_2O_2 concentration (Figure 5B). The two products were formed with constant rates during the peroxide titration, eliminating the possibility of multiple oxidations and showing that neither is intermediary of the other. Such an observation suggests that both products are derived directly from **5** via two, independent, nonprocessive enzymatic reactions. Regarding the overall chemical reactions, oxidative C−H bond cleavage and nonoxidative C−F bond cleavage differ by two electrons because fluorine leaves as an anion, implicating different mechanisms for the two reactivities. The most likely two-electron source for the C−F bond cleavage pathway would be the oxidation of H_2O_2 to oxygen (i.e., catalase-like activity) since more than 1 equiv of H_2O_2 was required to achieve complete conversion of **5** to **1a** (Figure 5A); therefore, the generation of **1a** and fluoride could be accompanied by oxygen generation.

To detect the possibility of O_2 formation, we employed an oxygen electrode to compare the O_2 formation rate between the natural substrate **1** and analogue **5** when they were mixed with LmbB2 at a saturated, 1 mM H_2O_2 concentration (Figure 5C). Without any organic substrate, LmbB2 shows a slow catalase activity of 0.9 s^{-1}. When the substrate concentration was increased, less oxygen was generated due to the hydroxylation reaction of **1** competing with the catalase activity. The loss of the catalase-like activity upon substrate addition was more pronounced for the natural substrate **1** versus the substrate analogue **5**, which reflects the more rapid

DOI: 10.1021/acscatal.9b00231
ACS Catal. 2019, 9, 4764−4776

Table 1. Distribution of the ^{18}O-Labeled Product(s) after the LmbB2 Reaction Using ^{18}O-enriched H_2O or H_2O_2[a]

	^{18}O atom %		hydroxylation			dehalogenation and hydroxylation		
substrate	water	peroxide	$^{16}O/^{16}O$	$^{16}O/^{18}O$	$^{18}O/^{18}O$	$^{16}O/^{16}O$	$^{16}O/^{18}O$	$^{18}O/^{18}O$
tyrosine		⩾90	7.2 ± 0.3	92.8 ± 0.3				
	88		87.7 ± 0.9	11.2 ± 0.8	1.0 ± 0.1			
3-fluoro-L-tyrosine		⩾90	15.5 ± 0.2	84.5 ± 0.2		30.3 ± 1.0	69.7 ± 1.0	
	88		57.3 ± 1.6	35.8 ± 1.6	6.9 ± 0.7	36.2 ± 0.9	51.5 ± 0.7	12.3 ± 1.2

[a]L-Tyrosine and 3-fluoro-L-tyrosine were used as the substrates in independent experiments. The standard deviation values were obtained from three replicate experiments.

reaction and consumption of H_2O_2 for hydroxylation of **1**. When substrate concentrations exceeded 200 μM, the rate of oxygen formation gradually approached 0 and 10 min^{-1} for **1** and **5**, respectively. This result suggests a hypothesis that H_2O_2 is the primary two-electron source in the C−F bond cleavage pathway. When LmbB2 reacts with **5** to continuously form **1a** and F^-, more than 1 equiv of H_2O_2 is reacted because it acts as both the oxygen source and the electron source in two half-reactions to bring the enzyme back to the resting state after each catalytic turnover.

After obtaining O_2 production during the catalytic turnover of **1** and **5**, we sought to model the catalase inhibition assays kinetically. For the case of **1**, the competition assay could be well described by a model in which **1** competes with H_2O_2 for the free enzyme (Scheme S1 and Figure S6). However, in the competition assay using **5**, the O_2 production rate did not approach zero, and the first model could not explain the catalytic behavior (Figure S6). Therefore, a second model which allows the production of DOPA concomitant with an oxidized enzyme was proposed to fit the change in the O_2 production rate of **5** (Scheme S2 and Figure S7). Currently, however, many of the microscopic rate constants for the reaction are unknown; thus, the modeling should be considered as qualitative rather than quantitative.

Source of Oxygen Determined by Isotope Labeling and Redox Potential Measurement. To determine the oxygen source of the added hydroxyl in the LmbB2-catalyzed reaction, isotope labeling studies were performed. Reactions were carried out with **1** and **5** in ^{18}O-enriched water (88% ^{18}O) or H_2O_2 (⩾90% ^{18}O). When ^{18}O-labeled H_2O_2 was used to react with **1** in normal ^{16}O-water, the product **1a** had over 90% enriched ^{18}O in the newly incorporated hydroxyl group (Figure 6A, left panel), which indicates that H_2O_2 is the source of the new oxygen atom. Similarly, when normal H_2O_2 in ^{18}O-labeled H_2O was used, 87.7% of the **1a** produced was not isotopically enriched with ^{18}O (Figure 6A, right panel). The 11.2% ^{18}O enrichment when labeled water was used derives from isotope scrambling presumably with either a substrate-based, possibly radical, intermediate or the heme iron bound oxygen responsible for O-atom transfer.

Similar reactions were performed using **5**, which yielded two products: **5a** through hydroxylation and **1a** via substitution of fluorine. When labeled peroxide was used, the majority of both products contained one ^{18}O atom, 84.5% and 69.7% (Figure 6B, left panel), respectively, similar to what was observed for **1**. Significantly more scrambling is observed when **5** was used as the substrate, presumably due to longer lifetimes of catalytic intermediates. When labeled water was used, the majority of **5a** produced was not enriched with ^{18}O ($^{16}O^{16}O$, 57.3%). However, significant scrambling was observed ($^{16}O^{18}O$, 35.8%), including doubly labeled **5a** ($^{18}O^{18}O$, 6.9%) (Figure 6B, right panel). Observation of a doubly labeled product implies that the aromatic 4-hydroxyl group becomes very active in at least one intermediate and can exchange with bulk water. The dehalogenation reaction of **5** to **1a** performed in labeled water showed the most significant degree of scrambling (Figure 6B, right panel), 51.5% singly labeled and 12.3% doubly labeled, presumably because it has the longest-lived intermediate(s). Nevertheless, observation of nonenriched **1a** (36.2%) in excess of the residual unlabeled water (12%, calculated ^{16}O percentage) and the majority of **1a** labeled when labeled peroxide was used confirms that the source of oxygen for the dehalogenation is indeed H_2O_2. The distribution of the ^{18}O-incorporated product(s) is summarized in Table 1. As a control, the unreacted substrates, **1** and **5**, remained as purely unlabeled in all reactions (Figure S8). To better understand the unusual reactivities for LmbB2 and explain the atypical C−H and C−F bond hydroxylation, we also performed Fe^{3+}/Fe^{2+} redox potential measurements with a dye-coupled assay.[27] LmbB2 and Nile Blue (E_m = −116 mV) were reduced by receiving electrons from xanthine/xanthine oxidase simultaneously (Figure S9A). The linear fitting of the Nernst plot indicated the redox potential of LmbB2 as −98 ± 2 mV at pH 7.0 and room temperature (Figure S9B). The determined redox potential value is at the high end of those reported for typical histidyl-ligated peroxidases (−250 to −100 mV) and higher than those of most thiolate-ligated heme enzymes (−340 to −6 mV).[28,29]

DISCUSSION

Previous work described the LmbB2 protein and its function.[11,17] The rigorous study of enzymatic activity on a variety of substrates resulted in a mechanistic understanding in this study. LmbB2 has been previously classified as a unique member of the peroxidase superfamily,[17] whose typical function is to oxidize organic and inorganic substrates by H_2O_2 and yield one-electron-oxidized products and water molecules. The data presented demonstrate that LmbB2 cleaves a C−H bond, or a C−X bond if it is present, during hydroxylation. A histidyl-ligated heme enzyme promoting hydroxylation is unusual, because such a catalytic function is commonly found in two superfamilies of enzymes, cytochrome P450s and peroxygenases, which both utilize a thiolate-ligated heme. Thus, there is a pressing need for a mechanistic understanding of the LmbB2-catalyzed reaction.

The observation of a histidyl-ligated heme enzyme to promote hydroxylation concomitant with both C−H and C−F bond cleavages is unprecedented. The aromatic C−F bond is believed to be one of the strongest bonds and thus is not easily dissociated.[30] Several synthetic nonheme iron complexes were reported to be able to perform C−F bond cleavage during oxygenation.[31−33] The cleavage of C−H and C−F bonds by a single biological iron center is also very rare. Such a reaction has been reported for nonheme iron-dependent thiol

DOI: 10.1021/acscatal.9b00231
ACS Catal. 2019, 9, 4764−4776

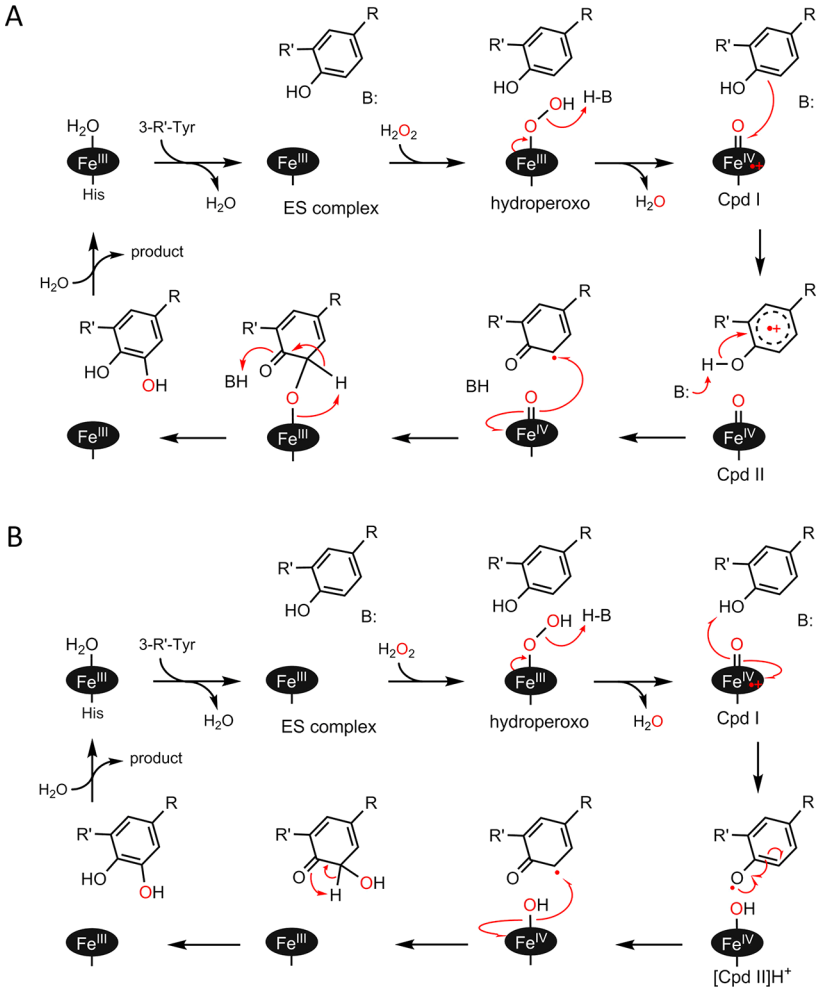

Figure 7. Proposed reaction pathway for LmbB2 hydroxylation. Oxidative aromatic C−H bond cleavage generates the product DOPA or its derivatives. A Compound I like intermediate performs electron transfer in this model (A). An alternative mechanism (B) like that of cytochrome P450 suggests that the Compound I like intermediate abstracts a hydrogen atom. R = main chain of the amino acid; R′ = H, NO_2, F, Cl, I.

dioxygenases working on a protein-based cofactor with only a single turnover.[34−36] Thiolate-ligated cytochrome P450s are well-known for hydroxylating aromatic C−H bonds;[37] however, hydroxylation of an aromatic C−F bond has only been reported for hexafluorobenzene or para-substituted anilines and phenols.[38,39] No histidyl-ligated heme enzymes have been reported for C−F bond hydroxylation, and certainly none for promoting both C−H and C−F bond hydroxylation with multiple turnovers as LmbB2 does.

The most relevant known example to this study is another histidyl-ligated heme enzyme, which catalyzes the two-electron oxidation of trihalophenols at the para position, resulting in quinone and halides.[40,41] Studies have shown that trifluorophenol had the least activity among all the halogenated substrates, and high-valent heme iron species oxidize substrate with water as the source of oxygen instead of peroxide.[42,43] In contrast, LmbB2 catalyzes oxidative C−H bond and non-oxidative C−X bond hydroxylation on the meta positions of L-tyrosine analogues to form quinol and halides using H_2O_2, and the fluoro-substituted tyrosine has the highest dehalogenation reactivity among all the halogenated substrates. Such differences indicate that the governing factor of the catalysis is distinct between LmbB2 and dehaloperoxidase. Thus, LmbB2 is unique for its chemistry, since it is the first example of substrate-based C−H and C−F bond hydroxylation by a histidyl-ligated heme enzyme with multiple turnovers.

The fluorinated compound **5** yielding the highest amount of dehalogenated product among halogen-substituted substrates is quite intriguing because a C−F bond is more durable than C−Cl and C−I bonds. Presumably, the small size of a fluorine atom allows the aromatic ring of L-tyrosine to access both binding orientations at the heme: i.e., fluorine can point toward or away from the heme center. Therefore, hydroxylation at both C3 and C5 of **5** would be possible. The formation of two hydroxylated products in LmbB2 reactions with **6** and **7** again indicates that the active site can accommodate the binding of L-tyrosine analogues with even larger halogen substituents in both possible orientations at the heme. However, the order of yield in **1a** (F > Cl > I) inversely reflects the order of the size of the halogen atoms (F < Cl < I). In addition to the binding affinities (F > Cl > I), one possible explanation is that the larger halogen atom favors binding in such a way that it is pointed away from the heme and, therefore, there is less of a chance to have the product of C−X hydroxylation. Additionally, the larger atom has a more significant steric effect, making the 5- position even less accessible for bond cleavage by the active heme species. Another plausible reason is that fluorine is the most electronegative of the halogens, which makes the adjacent

DOI: 10.1021/acscatal.9b00231
ACS Catal. 2019, 9, 4764−4776

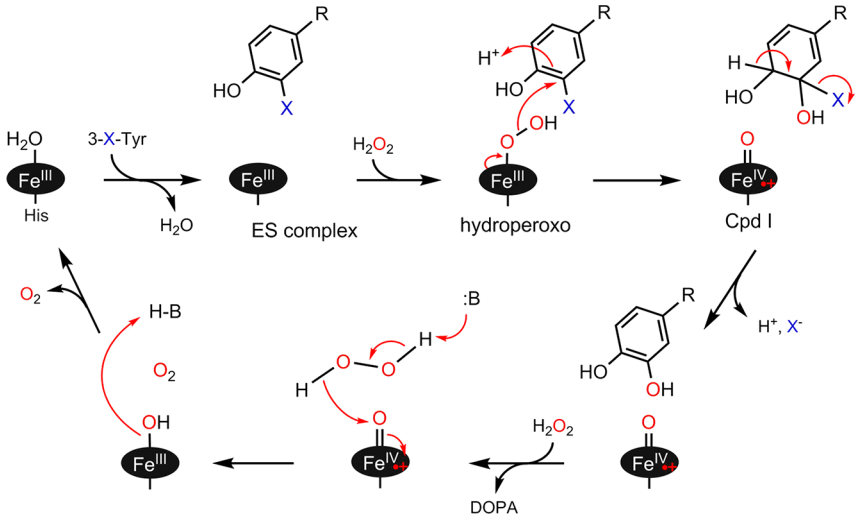

Figure 8. Proposed mechanistic model for the carbon−halogen (C−X) bond cleavage. The iron-bound hydroperoxo intermediate is proposed to perform aromatic nucleophilic substitution, leading to cleavage of the aromatic C−X bond with DOPA formation as the only hydroxylation product. The Compound I like intermediate subsequently performs a catalase-like reaction with O_2 liberation as a side product. R = main chain of amino acid; X = F, Cl, I.

carbon more electropositive and therefore more likely to undergo nucleophilic attack, ultimately generating **1a**. Therefore, the order of **1a** production (F > Cl > I) in the LmbB2 reaction is in accord with the order of electronegativity of halogen substituents (F > Cl > I).

Isotope ^{18}O labeling experiments with the reaction of **1** indisputably indicated that the oxygen source for normal hydroxylation comes from H_2O_2, while the intermediate in the natural reaction is short-lived with little chance to exchange with water molecules. Using **5** as the substrate, both defluorinated and hydroxylated products, **1a** and **5a**, have a significant scrambling effect and double ^{18}O incorporation even though H_2O_2 is still the oxygen source of hydroxylation on both of the C−H and C−F sites. The ^{18}O labeling study has provided important mechanistic insights into the LmbB2 pathways. The fact that 4-hydroxyl can exchange with water suggests that the aromaticity is broken during catalysis at a certain stage; a ketone intermediate is plausible.[44] The newly formed hydroxyl was also exchangeable in both hydroxylation and dehalogenation, which implies a substrate-based intermediate or the iron-bound oxygen that is responsible for O atom transfer. The reaction with **5** was slow, in comparison to **1**, by the fluorine substituent, and future attempts to capture intermediates under certain conditions may be possible. Finally, together with the findings of consumption of more than 1 equiv of peroxide and generation of fluoride and oxygen during the C−F bond cleavage with multiple turnovers, we proposed two separate mechanistic pathways for C3 versus C5 hydroxylation of L-tyrosine derivatives.

When the functional group points away from the heme center, hydroxylation occurs via the usual mechanism (Figure 7A). We propose that, after organic substrate binding, peroxide binds to the ferric heme center and forms a histidyl-ligated Compound I (Cpd I, an iron(IV) oxo porphyrin cation radical) like species, which receives one electron from the tyrosine or the reactive analogues as the first step of the substrate oxidation. Initiating the reaction by one-electron oxidation may be preferred because histidyl-ligated hemes are typically considered competent for binding oxygen or electron transfer. However, its capacity to directly abstract a hydrogen atom like thiolate-ligated heme is questionable.[45−47] The Cpd I species will be reduced to a deprotonated Compound II (Cpd II, an iron(IV) oxo porphyrin), after one-electron transfer to generate a tyrosyl cation radical. A nearby active-site base could easily deprotonate the tyrosyl cation radical due to the dramatically decreased pK_a of the tyrosyl cation radical in comparison with tyrosine.[48] Then, the ferryl-oxo group attacks the radical, generating an intermediate-bound adduct and finally forming the derivative DOPA products.

An alternate reaction pathway is also proposed (Figure 7B), in which the Cpd I-like intermediate would directly abstract an H atom from the 4-hydroxyl, like most P450s do, to generate protonated Cpd II and a substrate-based tyrosyl radical; the radical will migrate to C5, resulting in a ketone-based tyrosyl radical. The Cpd II like intermediate then proceeds with hydroxyl radical rebound to the C5 position and finally forms the hydroxylated product after a rearrangement. More mechanistic studies are necessary to reveal the potential of histidyl-ligated heme for hydroxylation and discriminate between these two mechanisms. Nevertheless, we propose that a quinone radical is a crucial substrate-based intermediate of the catalytic pathway on the basis of the data from the unreactive analogues **2** and **3** and the scrambling result from isotope labeling.

Since halogens are electronegative, C3 is partially electropositive in **5**−**7**. Therefore, ferric heme-bound hydroperoxide can perform a nucleophilic attack at C3 once they are close enough, generating a high-valent heme species. Fluoride then leaves the ring to create a rearomatized product, DOPA (Figure 8). The resulting Cpd I-like species can either activate another molecule of the organic substrate or react with another 1 equiv of H_2O_2 to return to the resting state via catalase-like activity, which likely precludes the possibility for the leaving halide to bind to the heme Fe to inactivate the enzyme. Our kinetic modeling (Scheme S2) suggests that organic substrates are unable to compete with H_2O_2 for the Cpd I like species effectively. A flavin-dependent monooxygenase was proposed to achieve dehalogenation while forming a quinone via an electrophilic aromatic substitution (EAS) mechanism.[49] While an electrophilic substitution mechanism cannot be positively

DOI: 10.1021/acscatal.9b00231
ACS Catal. 2019, 9, 4764−4776

excluded in LmbB2 without further experimental evidence, the formation of quinol and F^- favors a nucleophilic substitution mechanism because the products are reduced by two electrons in comparison to the EAS mechanism. Further, the fluorinated phenol ring is relatively electron deficient and would make a weak nucleophile. The natural substrate of LmbB2 has a neutral C3, which makes C−H bond cleavage proceeding from nucleophilic attack very unlikely; however, the inductive effect caused by an electronegative group at C3 makes a nucleophilic attack at this position more likely, and nucleophilic substitution of fluorinated aromatics is common in organic chemistry.[50,51] Altogether, the steric effect and inductive effect of the halogen substituent distribute the substrate between two distinct reaction pathways.

The fluorine substituents on substrate-like molecules are often considered when developing new drug candidates. Due to their unique steric and lipophilic properties, among others,[52−54] halogenated compounds have now been widely used against a large number of biomedically essential targets. Our findings here call attention to the reality that enzymes, especially metalloenzymes, are often powerful enough to cleave off the covalently bound halogens and, therefore, destroy such intentionally designed halogenated drugs. However, these findings may also be used to help develop new catalysts to mitigate the potential health threats of halogenated aromatic hydrocarbons (HAHs) that contaminate the natural environment as an unintended and undesired effect of civilization. HAHs are not only significant contaminants of the air, drinking water, and sediment but also have been linked to cardiotoxicity and the DNA damage that leads to cancer due to inherent reactivity, such as aryl hydrocarbon receptor activation.[55−57] Designing catalysts and engineering biosystems capable of degrading such toxic and fatal HAHs have long been goals of scientists,[41,58−60] and most catalysts activate C−Cl, C−Br, or C−I bonds but have very little or no reactivity on C−F bonds. However, LmbB2 reported here has precisely the opposite activation tendency, where defluorination is actually the most efficient process and only requires the inexpensive oxidant H_2O_2, which provides a potential new scaffold for engineering enzymatic degradation of HAHs, especially fluorinated aromatics, through hydroxylation of the carbon−halogen bonds.

CONCLUSION

This study shows that the histidyl-ligated, heme-dependent L-tyrosine hydroxylase LmbB2 has a wide range of catalytic activities toward deactivated L-tyrosine analogues, as long as the 4-hydroxyl group is present. The monosubstituted tyrosine analogues represented by 3-fluoro-L-tyrosine presumably bind in two different orientations at the heme active site, substituents pointing away from or toward the heme center. The former orientation results in an oxidative C−H bond cleavage at C5, while the latter allows for different chemistry to happen on C3; for example, the carbon−fluorine bond hydroxylation to generate DOPA. On the basis of spectroscopic characterization and product analysis, we proposed two distinct pathways to explain how LmbB2 accomplishes the catalytic reaction upon different substrate orientations. The surprisingly robust heme oxidant of LmbB2 sheds new light on the capacity for heme enzymes to perform a wide range of chemistries. Finally, this study is the first to describe a biocatalytic C−H and C−F bond cleavage through hydroxylation at the carbon site promoted by a histidyl-ligated heme enzyme. This finding broadens our understanding of fluorine chemistry and provides potentially novel medicinal and environmental applications for hemoproteins.

MATERIALS AND METHODS

Chemicals. L-Tyrosine and all of the analogues were purchased with the highest purity as listed below: **1**, Alfa Aesar, 99%; **2**, Acros Organics, 98.5%; **3**, Sigma-Aldrich, 98%; **4**, Sigma-Aldrich, crystalline; **5**, TCI, 98%; **6**, Sigma-Aldrich, 97%; **7**, Alfa Aesar, 98%; *N*-boc-L-tyrosine, Sigma-Aldrich, 98%; *p*-Cresol, Sigma-Aldrich, 99%. Stock solutions were made in 0.1 M HCl.

Enzyme Overexpression and Purification. LmbB2 from *Streptomyces lincolnensis* with a His_6-tag at the N-terminus cloned into a pET16 plasmid with ampicillin resistance was a generous gift from Prof. Wolfgang Piepersberg (Mikrobiologie, Bergische Universität GH Wuppertal, Germany). pET16B2 was transformed into an *E. coli* BL21 (DE3) overexpression system. Expression of LmbB2 was started in Luria−Bertani (LB) medium with 100 μg/mL ampicillin at 37 °C. At an $OD_{600\,nm}$ value of 0.3, δ-aminolevulinic acid and ferrous ammonium sulfate were added to a final concentrations of 20 and 10 mg per liter of culture, respectively. The cells were induced at an $OD_{600\,nm}$ value of 0.6 using a final concentration of 0.5 mM isopropyl-β-D-thiogalactopyranoside (IPTG) with continued incubation overnight at 28 °C and 220 rpm agitation. The cells were harvested 12 h after IPTG induction by centrifuging at 6000*g* for 20 min at 4 °C.

To isolate LmbB2, the cells were resuspended in buffer A (50 mM KPi buffer with 200 mM NaCl at pH 8) supplemented with 1 mM PMSF protease inhibitor and DNase I (0.05 mg/mL) and lysed using a Microfluidizer LM20 cell disruptor. The supernatant was recovered after centrifugation (27000*g*, 4 °C for 30 min) and applied to a Ni-affinity column pre-equilibrated with buffer A. LmbB2 was eluted by a gradient profile using buffers A and B (50 mM KPi buffer with 200 mM NaCl, 500 mM imidazole at pH 8). The eluted protein was collected and concentrated using an Amicon centrifugal filter (Ultra-15 10K, Millipore) and then desalted into 50 mM KPi pH 8 and 50 mM NaCl with additional 5% glycerol using a Sephadex G-25 column (GE Healthcare) and stored at −80 °C for future use.

Catalytic Reaction Setup and HPLC Analyses. The standard HPLC assays were conducted at room temperature in 100 mM KPi with 50 mM NaCl at pH 8. A portion of 100 μM enzyme was incubated with 3 mM L-tyrosine or analogues for 5 min prior to H_2O_2 addition. To avoid any heme bleaching, a 20 mM H_2O_2 stock solution was titrated to initiate the reaction by adding multiple small volumes each time until a final concentration of 3 mM was reached. Enzymatic assays and controls conducted were of four types: (i) 100 μM enzyme, 3 mM substrate, and 3 mM H_2O_2 and three controls with (ii) 100 μM enzyme and 3 mM substrate, (iii) 3 mM substrate and 3 mM H_2O_2, and (iv) 100 μM enzyme and 3 mM H_2O_2. For **2** and **3**, a concentration of up to 20 mM at pH 7−10 (out of this range, the enzyme became unstable) and two oxidants (H_2O_2 and peracetic acid) were examined. After reaction for 10 min, 10 μL of 6 M HCl was used to quench the reaction. The final volume for each reaction/control was 200 μL. After the precipitant was removed by centrifugation, the supernatant was filtered using a 10 kDa molecular weight cutoff centrifugal filter unit (Millipore). A 10 μL portion of filtrate was injected into an InertSustain C18 column (5 μm particle size, 4.6 × 100

DOI: 10.1021/acscatal.9b00231
ACS Catal. 2019, 9, 4764−4776

mm, GL Sciences Inc.) and then analyzed by a Thermo Scientific Ultimate-3000SD HPLC rapid separation system equipped with a photodiode array detector. The UV−vis spectra were recorded at full range from 190 to 800 nm. The HPLC method was derived from a published method using an isocratic elution profile (3/97/0.1, ACN/H_2O/FA).[61] All of the HPLC profiles are shown with absorbance at 280 nm except assays for **2**, which were at both 257 and 280 nm. The peaks eluted from HPLC were then collected and concentrated by SpeedVac (ThermoFisher) for further MS and NMR analysis.

Isothermal Titration Calorimetry (ITC) Measurements. A Microcal VP-ITC system (Malvern Instruments) was used to conduct the ITC measurements as previously described.[62] The titration buffer consisted of 100 mM KPi with 50 mM NaCl at pH 8. L-Tyrosine or analogues were prepared in titration buffer and injected into a cell containing 2 mL of 100−120 μM purified enzyme. Binding of L-tyrosine and its analogues was assessed in a total volume of 300 μL at the following concentrations: 1.5 mM **1**, 10 mM **2**, and 20 mM **3**. After the temperature was equilibrated to 20 °C, a total of 50 injections were performed with a reference power of 15 μcal/s and a stirring speed of 350 rpm. The ITC data were processed and analyzed using nonlinear least-squares curve fitting of one-site binding models with Origin version 7.0 (OriginLab Corp.) software.

Electron Paramagnetic Resonance (EPR) Analysis on Nitrosyl Complex. Ferrous heme enzyme was made by reducing 200 μM argon-saturated enzyme with 1 mM sodium dithionite anaerobically. The argon-saturated enzyme was prepared using the published method.[22] Reduced LmbB2 was exposed to excess NO released by diethylamine NONOate (Cayman) in a sealed O_2-free vial. Substrate **1**, analogues **2** and **3**, and unbound phenols *N*-boc-L-tyrosine and *p*-cresol were added with a final concentration of 20 mM. All samples were frozen in 4 mm quartz EPR tubes by liquid nitrogen. X-band EPR spectra were recorded by a Bruker E560 spectrometer at 9.4 GHz microwave frequency with an SHQE-W resonator at 100 kHz modulation frequency equipped with a cryogen-free 4 K temperature system as described earlier.[63] Spectra for nitrosyl samples were collected at 50 K and 0.05 mW power. The *g* values reported were obtained by inspection of the EPR line shape.

High-Resolution Mass Spectrometry. Mass spectra were collected on a maXis plus quadrupole time of flight mass spectrometer equipped with an electrospray ionization source (Bruker Daltonics) and operated in the positive ionization mode. Samples were introduced via a syringe pump at a constant flow rate of 3 μL/min. Instrumental parameters used were standard preset values for small molecules. Important parameters are summarized as follows: capillary voltage, 3500 V with a set end plate offset of 500 V; nebulizer gas pressure, 0.4 bar; dry gas flow rate, 4.0 L/min; source temperature, 200 °C; quadrupole ion energy, 3.0 eV; collision energy, 5.0 eV. Scans were collected at a rate of one scan per second in the range of $50 \leqslant m/z \leqslant 1500$, and 60 s of data were averaged to yield a final spectrum. Compass Data Analysis software version 4.3 (Bruker Daltonics) was used to process all mass spectra.

^{1}H and ^{19}F Nuclear Magnetic Resonance (NMR) Spectroscopy. ^{1}H and ^{19}F NMR spectra were recorded on a Bruker (Billerica, MA) Avance III HD 500 MHz spectrometer equipped with a 5 mm Cryoprobe Prodigy apparatus at 300 K. Spectra were recorded in 90/10 buffer/D_2O. One-dimensional ^{1}H spectra (zg30) were recorded with 1 s relaxation delay and 32k data points and multiplied with an exponential function for a line broadening of 0.3 Hz before Fourier transformation. One-dimensional ^{1}H-coupled ^{19}F spectra (zgflqn) were recorded with a 5 s relaxation delay and 128k data points and multiplied with an exponential function for a line broadening of 5 Hz before Fourier transformation and referenced to internal trifluoroacetic acid (−76.5 ppm). Each peroxide concentration dependent ^{19}F NMR spectrum was recorded with 64 scans. All NMR data were processed using MestReNova NMR v11.0.3 software. The detailed NMR data are reported in the Supporting Information.

Oxygen Determination. An oxygen electrode (Oxygraph, Hansatech Instruments) was used to measure the oxygen production in LmbB2 reactions with substrate **1** or **5** at room temperature. A total reaction volume of 1 mL consisted of 0.5−2 μM enzyme, 1 mM H_2O_2, and various concentrations of substrate (0−0.65 mM) in 50 mM KPi with 50 mM NaCl at pH 8. The enzyme was preincubated with the substrate in a sealed electrode chamber with constant stirring. The reaction was initiated by addition of H_2O_2 into the electrode chamber. Heated denatured enzyme reacting with peroxide was used as a blank for subtraction. Substrate concentration was recorded as [S], enzyme concentration was recorded as [E], and oxygen production rate was recorded as ΔO_2. The oxygen production rate per unit of enzyme ΔO_2/[E] versus [S] was plotted to compare the difference between substrates **1** and **5**. The detailed fitting procedure is shown in the Supporting Information.

Redox Potential Determination. The method of redox potential measurement was derived from a reported method for determination of redox potential in heme proteins.[27] The assay contained 6 μM LmbB2, 300 μM xanthine, and 40 μM Nile Blue in 1 mL of anaerobic 100 mM KPi at pH 7.0 at room temperature. A 50 nM portion of xanthine oxidase was added to initiate the reduction, and UV−vis spectra were recorded every 30 s for 25 min. A 5 mM portion of dithionite was added at the end to obtain a fully reduced spectrum. Absorbance changes corresponding to heme and dye reduction were measured at 404 and 636 nm. The potential was given versus a normal hydrogen electrode.

■ ASSOCIATED CONTENT

Supporting Information

The Supporting Information is available free of charge on the ACS Publications website at DOI: 10.1021/acscatal.9b00231.

ITC binding experimental data of tyrosine analogues, LmbB2 reaction profiles with L-phenylalanine, *O*-methyl-L-tyrosine, 3-chloro-L-tyrosine, and 3-iodo-L-tyrosine, EPR spectra of E-NO$^\bullet$ complex alone and with unbound phenols, kinetic modeling of L-tyrosine and 3-fluoro-L-tyrosine competing with catalase activity of LmbB2, LmbB2 redox potential measurement, NMR data for substrate analogs and products, and MS analysis of isotope labeling reaction with unreacted substrates (PDF)

■ AUTHOR INFORMATION

Corresponding Author

*A.L.: tel, +1-210-458-7062; fax, 210-458-7428; e-mail, Feradical@utsa.edu; web, http://Feradical.utsa.edu.

DOI: 10.1021/acscatal.9b00231
ACS Catal. 2019, 9, 4764−4776

ORCID

Yifan Wang: 0000-0003-0378-2469
Ian Davis: 0000-0002-1566-4972
Inchul Shin: 0000-0001-8111-8948
Daniel J. Wherritt: 0000-0002-8616-9864
Wendell P. Griffith: 0000-0003-2633-6103
Kednerlin Dornevil: 0000-0003-2451-6661
Aimin Liu: 0000-0002-4182-8176

Notes

The authors declare no competing financial interest.

■ ACKNOWLEDGMENTS

We thank Dr. Jie Hu for participating in the *O*-methyl-L-tyrosine reaction analysis. This work was financially supported by a National Institutes of Health (NIH) grant GM108988 (to A.L.), National Science Foundation (NSF) grants CHE-1708237 (to K.L.C.) and CHE-1808637 (to A.L.), and the Lutcher Brown Endowment fund (to A.L.). The mass spectrometry facility was sponsored by National Institutes of Health grant G12MD007591. The NMR facility was sponsored by the National Science Foundation (NSF) under award no. 1625963.

■ REFERENCES

(1) Ullrich, R.; Hofrichter, M. Enzymatic Hydroxylation of Aromatic Compounds. *Cell. Mol. Life Sci.* **2007**, *64*, 271−293.
(2) Zanger, U. M.; Schwab, M. Cytochrome P450 Enzymes in Drug Metabolism: Regulation of Gene Expression, Enzyme Activities, and Impact of Genetic Variation. *Pharmacol. Ther.* **2013**, *138*, 103−141.
(3) Sono, M.; Roach, M. P.; Coulter, E. D.; Dawson, J. H. Heme-Containing Oxygenases. *Chem. Rev.* **1996**, *96*, 2841−2887.
(4) Fitzpatrick, P. F. Mechanism of Aromatic Amino Acid Hydroxylation. *Biochemistry* **2003**, *42*, 14083−14091.
(5) Leahy, J. G.; Batchelor, P. J.; Morcomb, S. M. Evolution of the Soluble Diiron Monooxygenases. *FEMS Microbiol. Rev.* **2003**, *27*, 449−479.
(6) Rosenzweig, A. C.; Sazinsky, M. H. Structural Insights into Dioxygen-activating Copper Enzymes. *Curr. Opin. Struct. Biol.* **2006**, *16*, 729−735.
(7) Sariaslani, F. S. Microbial Enzymes for Oxidation of Organic-Molecules. *Crit. Rev. in Biotechnol.* **1989**, *9*, 171−257.
(8) Colabroy, K. L. Tearing Down to Build Up: Metalloenzymes in the Biosynthesis Lincomycin, Hormaomycin and the Pyrrolo[1,4]-benzodiazepines. *Biochim. Biophys. Acta, Proteins Proteomics* **2016**, *1864*, 724−737.
(9) Peschke, U.; Schmidt, H.; Zhang, H. Z.; Piepersberg, W. Molecular Characterization of the Lincomycin-Production Gene Cluster of *Streptomyces lincolnensis* 78−11. *Mol. Microbiol.* **1995**, *16*, 1137−1156.
(10) Hofer, I.; Crusemann, M.; Radzom, M.; Geers, B.; Flachshaar, D.; Cai, X. F.; Zeeck, A.; Piel, J. Insights into the Biosynthesis of Hormaomycin, an Exceptionally Complex Bacterial Signaling Metabolite. *Chem. Biol.* **2011**, *18*, 381−391.
(11) Connor, K. L.; Colabroy, K. L.; Gerratana, B. A Heme Peroxidase with a Functional Role as an L-Tyrosine Hydroxylase in the Biosynthesis of Anthramycin. *Biochemistry* **2011**, *50*, 8926−8936.
(12) Li, W.; Chou, S.; Khullar, A.; Gerratana, B. Cloning and Characterization of the Biosynthetic Gene Cluster for Tomaymycin, an SJG-136 Monomeric Analog. *Appl. Environ. Microbiol.* **2009**, *75*, 2958−2963.
(13) Li, W.; Khullar, A.; Chou, S.; Sacramo, A.; Gerratana, B. Biosynthesis of Sibiromycin, a Potent Antitumor Antibiotic. *Appl. Environ. Microbiol.* **2009**, *75*, 2869−2878.
(14) Najmanova, L.; Ulanova, D.; Jelinkova, M.; Kamenik, Z.; Kettnerova, E.; Koberska, M.; Gazak, R.; Radojevic, B.; Janata, J. Sequence Analysis of Porothramycin Biosynthetic Gene Cluster. *Folia Microbiol. (Dordrecht, Neth.)* **2014**, *59*, 543−552.
(15) Brahme, N. M.; Gonzalez, J. E.; Rolls, J. P.; Hessler, E. J.; Mizsak, S.; Hurley, L. H. Biosynthesis of the Lincomycins. 1. Studies Using Stable Isotopes on the Biosynthesis of the Propyl- and Ethyl-L-Hygric Acid Moieties of Lincomycin A and B. *J. Am. Chem. Soc.* **1984**, *106*, 7873−7878.
(16) Zhong, G.; Zhao, Q.; Zhang, Q.; Liu, W. 4-Alkyl-L-(dehydro)proline Biosynthesis in Actinobacteria Involves N-terminal Nucleophile-Hydrolase Activity of γ-Glutamyltranspeptidase Homolog for C-C Bond Cleavage. *Nat. Commun.* **2017**, *8*, 16109.
(17) Novotna, J.; Olsovska, J.; Novak, P.; Mojzes, P.; Chaloupkova, R.; Kamenik, Z.; Spizek, J.; Kutejova, E.; Mareckova, M.; Tichy, P.; Damborsky, J.; Janata, J. Lincomycin Biosynthesis Involves a Tyrosine Hydroxylating Heme Protein of an Unusual Enzyme Family. *PLoS One* **2013**, *8*, e79974.
(18) Poulos, T. L. The Role of the Proximal Ligand in Heme Enzyme. *JBIC, J. Biol. Inorg. Chem.* **1996**, *1*, 356−359.
(19) Wang, X.; Peter, S.; Ullrich, R.; Hofrichter, M.; Groves, J. T. Driving Force for Oxygen-Atom Transfer by Heme-Thiolate Enzymes. *Angew. Chem., Int. Ed.* **2013**, *52*, 9238−9241.
(20) Guengerich, F. P. Mechanisms of Cytochrome P450-Catalyzed Oxidations. *ACS Catal.* **2018**, *8*, 10964−10976.
(21) Hayashi, T.; Hilvert, D.; Green, A. P. Engineered Metalloenzymes with Non-Canonical Coordination Environments. *Chem. - Eur. J.* **2018**, *24*, 11821−11830.
(22) Fu, R.; Liu, F.; Davidson, V. L.; Liu, A. Heme Iron Nitrosyl Complex of MauG Reveals an Efficient Redox Equilibrium between Hemes with Only One Heme Exclusively Binding Exogenous Ligands. *Biochemistry* **2009**, *48*, 11603−11605.
(23) Yonetani, T.; Yamamoto, H.; Erman, J. E.; Leigh, J. S.; Reed, G. H. Electromagnetic Properties of Hemoproteins V. Optical and Electron Paramagnetic Resonance Characteristics of Nitric Oxide Derivatives of Metalloporphyrin-Apohemoprotein Complexes. *J. Biol. Chem.* **1972**, *247*, 2447−2455.
(24) Wang, C.; Chen, S.; Caceres-Cortes, J.; Huang, R. Y.; Tymiak, A. A.; Zhang, Y. Chromatography-Based Methods for Determining Molar Extinction Coefficients of Cytotoxic Payload Drugs and Drug Antibody Ratios of Antibody Drug Conjugates. *J. Chromatogr. A* **2016**, *1455*, 133−139.
(25) Waite, J. H.; Andersen, S. O. 3,4-Dihydroxyphenylalanine (Dopa) and Sclerotization of Periostracum in *Mytilus edulis L. Biol. Bull.* **1980**, *158*, 164−173.
(26) Seyedsayamdost, M. R.; Yee, C. S.; Stubbe, J. Site-Specific Incorporation of Fluorotyrosines into the R2 Subunit of *E. coli* Ribonucleotide Reductase by Expressed Protein Ligation. *Nat. Protoc.* **2007**, *2*, 1225−1235.
(27) Efimov, I.; Parkin, G.; Millett, E. S.; Glenday, J.; Chan, C. K.; Weedon, H.; Randhawa, H.; Basran, J.; Raven, E. L. A Simple Method for the Determination of Reduction Potentials in Heme Proteins. *FEBS Lett.* **2014**, *588*, 701−704.
(28) Papadopoulou, N. D.; Mewies, M.; McLean, K. J.; Seward, H. E.; Svistunenko, D. A.; Munro, A. W.; Raven, E. L. Redox and Spectroscopic Properties of Human Indoleamine 2,3-Dioxygenase and a His303Ala Variant: Implications for Catalysis. *Biochemistry* **2005**, *44*, 14318−14328.
(29) Reedy, C. J.; Elvekrog, M. M.; Gibney, B. R. Development of a Heme Protein Structure-Electrochemical Function Database. *Nucleic Acids Res.* **2007**, *36*, D307−313.
(30) Blanksby, S. J.; Ellison, G. B. Bond Dissociation Energies of Organic Molecules. *Acc. Chem. Res.* **2003**, *36*, 255−263.
(31) Sahu, S.; Zhang, B.; Pollock, C. J.; Durr, M.; Davies, C. G.; Confer, A. M.; Ivanovic-Burmazovic, I.; Siegler, M. A.; Jameson, G. N.; Krebs, C.; Goldberg, D. P. Aromatic C-F Hydroxylation by Nonheme Iron(IV)-Oxo Complexes: Structural, Spectroscopic, and Mechanistic Investigations. *J. Am. Chem. Soc.* **2016**, *138*, 12791−12802.
(32) Sahu, S.; Quesne, M. G.; Davies, C. G.; Durr, M.; Ivanovic-Burmazovic, I.; Siegler, M. A.; Jameson, G. N.; de Visser, S. P.;

DOI: 10.1021/acscatal.9b00231
ACS Catal. 2019, 9, 4764−4776

Goldberg, D. P. Direct Observation of a Nonheme Iron(IV)-Oxo Complex that Mediates Aromatic C-F Hydroxylation. *J. Am. Chem. Soc.* **2014**, *136*, 13542−13545.
(33) de Ruiter, G.; Carsch, K. M.; Takase, M. K.; Agapie, T. Selectivity of C-H versus C-F Bond Oxygenation by Homo- and Heterometallic Fe_4, Fe_3 Mn, and Mn_4 Clusters. *Chem. - Eur. J.* **2017**, *23*, 10744−10748.
(34) Li, J.; Griffith, W. P.; Davis, I.; Shin, I.; Wang, J.; Li, F.; Wang, Y.; Wherritt, D. J.; Liu, A. Cleavage of a Carbon-Fluorine Bond by an Engineered Cysteine Dioxygenase. *Nat. Chem. Biol.* **2018**, *14*, 853−860.
(35) Wang, Y.; Griffith, W. P.; Li, J.; Koto, T.; Wherritt, D. J.; Fritz, E.; Liu, A. Cofactor Biogenesis in Cysteamine Dioxygenase: C-F Bond Cleavage with Genetically Incorporated Unnatural Tyrosine. *Angew. Chem., Int. Ed.* **2018**, *57*, 8149−8153.
(36) Li, J.; Koto, T.; Davis, I.; Liu, A. Probing the Tyr-Cys Cofactor Biogenesis in Cysteine Dioxygenase by the Genetic Incorporation of Fluorotyrosine. *Biochemistry* **2019**, DOI: 10.1021/acs.biochem.9b00006.
(37) Ortiz de Montellano, P. R. Hydrocarbon Hydroxylation by Cytochrome P450 Enzymes. *Chem. Rev.* **2010**, *110*, 932−948.
(38) Hackett, J. C.; Sanan, T. T.; Hadad, C. M. Oxidative Dehalogenation of Perhalogenated Benzenes by Cytochrome P450 Compound I. *Biochemistry* **2007**, *46*, 5924−5940.
(39) Cnubben, N. H.; Vervoort, J.; Boersma, M. G.; Rietjens, I. M. The Effect of Varying Halogen Substituent Patterns on the Cytochrome P450 Catalysed Dehalogenation of 4-Halogenated Anilines to 4-Aminophenol Metabolites. *Biochem. Pharmacol.* **1995**, *49*, 1235−1248.
(40) Feducia, J.; Dumarieh, R.; Gilvey, L. B.; Smirnova, T.; Franzen, S.; Ghiladi, R. A. Characterization of Dehaloperoxidase Compound ES and Its Reactivity with Trihalophenols. *Biochemistry* **2009**, *48*, 995−1005.
(41) Yin, L.; Yuan, H.; Liu, C.; He, B.; Gao, S.; Wen, G.; Tan, X.; Lin, Y. A Rationally Designed Myoglobin Exhibits a Catalytic Dehalogenation Efficiency More than 1000-Fold That of a Native Dehaloperoxidase. *ACS Catal.* **2018**, *8*, 9619−9624.
(42) Osborne, R. L.; Coggins, M. K.; Raner, G. M.; Walla, M.; Dawson, J. H. The Mechanism of Oxidative Halophenol Dehalogenation by *Amphitrite ornata* Dehaloperoxidase is Initiated by H_2O_2 Binding and Involves two Consecutive One-Electron Steps: Role of Ferryl Intermediates. *Biochemistry* **2009**, *48*, 4231−4238.
(43) Davis, M. F.; Gracz, H.; Vendeix, F. A.; de Serrano, V.; Somasundaram, A.; Decatur, S. M.; Franzen, S. Different Modes of Binding of Mono-, Di-, and Trihalogenated Phenols to the Hemoglobin Dehaloperoxidase from *Amphitrite ornata*. *Biochemistry* **2009**, *48*, 2164−2172.
(44) Murphy, R. C.; Clay, K. L. Preparation of Labeled Molecules by Exchange with Oxygen-18 water. *Methods Enzymol.* **1990**, *193*, 338−348.
(45) Poulos, T. L. Heme Enzyme Structure and Function. *Chem. Rev.* **2014**, *114*, 3919−3962.
(46) Yosca, T. H.; Behan, R. K.; Krest, C. M.; Onderko, E. L.; Langston, M. C.; Green, M. T. Setting an Upper Limit on the Myoglobin Iron(IV)hydroxide pK(a): Insight into Axial Ligand Tuning in Heme Protein Catalysis. *J. Am. Chem. Soc.* **2014**, *136*, 9124−9131.
(47) Rydberg, P.; Sigfridsson, E.; Ryde, U. On the Role of the Axial Ligand in Heme Proteins: A Theoretical Study. *J. Biol. Inorg. Chem.* **2004**, *9*, 203−223.
(48) Dixon, W. T.; Murphy, D. Determination of the Acidity Constants of Some Phenol Radical Cations by Means of Electron Spin Resonance. *J. Chem. Soc., Faraday Trans. 2* **1976**, *72*, 1221−1230.
(49) Pimviriyakul, P.; Surawatanawong, P.; Chaiyen, P. Oxidative Dehalogenation and Denitration by a Flavin-Dependent Monooxygenase Is Controlled by Substrate Deprotonation. *Chem. Sci.* **2018**, *9*, 7468−7482.
(50) Garcia, J.; Sorrentino, J.; Diller, E. J.; Chapman, D.; Woydziak, Z. R. A General Method for Nucleophilic Aromatic Substitution of Aryl Fluorides and Chlorides with Dimethylamine using Hydroxide-Assisted Decomposition of N,N-Dimethylforamide. *Synth. Commun.* **2016**, *46*, 475−481.
(51) Ajenjo, J.; Greenhall, M.; Zarantonello, C.; Beier, P. Synthesis and Nucleophilic Aromatic Substitution of 3-Fluoro-5-Nitro-1-(entafluorosulfanyl)benzene. *Beilstein J. Org. Chem.* **2016**, *12*, 192−197.
(52) Hernandes, M. Z.; Cavalcanti, S. M.; Moreira, D. R.; de Azevedo Junior, W. F.; Leite, A. C. Halogen Atoms in the Modern Medicinal Chemistry: Hints for the Drug Design. *Curr. Drug Targets* **2010**, *11*, 303−314.
(53) Wilcken, R.; Zimmermann, M. O.; Lange, A.; Joerger, A. C.; Boeckler, F. M. Principles and Applications of Halogen Bonding in Medicinal Chemistry and Chemical Biology. *J. Med. Chem.* **2013**, *56*, 1363−1388.
(54) Lu, Y.; Liu, Y.; Xu, Z.; Li, H.; Liu, H.; Zhu, W. Halogen Bonding for Rational Drug Design and New Drug Discovery. *Expert Opin. Drug Discovery* **2012**, *7*, 375−383.
(55) Heid, S. E.; Walker, M. K.; Swanson, H. I. Correlation of Cardiotoxicity Mediated by Halogenated Aromatic Hydrocarbons to Aryl Hydrocarbon Receptor Activation. *Toxicol. Sci.* **2001**, *61*, 187−196.
(56) Sun, J. L.; Zeng, H.; Ni, H. G. Halogenated Polycyclic Aromatic Hydrocarbons in the Environment. *Chemosphere* **2013**, *90*, 1751−1759.
(57) Fu, P. P.; Xia, Q.; Sun, X.; Yu, H. Phototoxicity and Environmental Transformation of Polycyclic Aromatic Hydrocarbons (PAHs)-Light-Induced Reactive Oxygen Species, Lipid Peroxidation, and DNA Damage. *J. Environ. Sci. Health. C: Environ. Carcinog. Ecotoxicol. Rev.* **2012**, *30*, 1−41.
(58) Sakamoto, H.; Imai, J.; Shiraishi, Y.; Tanaka, S.; Ichikawa, S.; Hirai, T. Photocatalytic Dehalogenation of Aromatic Halides on Ta_2O_5-Supported Pt−Pd Bimetallic Alloy Nanoparticles Activated by Visible Light. *ACS Catal.* **2017**, *7*, 5194−5201.
(59) Liao, R.; Chen, S.; Siegbahn, P. E. M. Which Oxidation State Initiates Dehalogenation in the B_{12}-Dependent Enzyme NpRdhA: Co^{II}, Co^{I}, or Co^{0}? *ACS Catal.* **2015**, *5*, 7350−7358.
(60) Ma, X.; Liu, S.; Liu, Y.; Gu, G.; Xia, C. Comparative Study on Catalytic Hydrodehalogenation of Halogenated Aromatic Compounds over Pd/C and Raney Ni Catalysts. *Sci. Rep.* **2016**, *6*, 25068.
(61) Olsovska, J.; Novotna, J.; Flieger, M.; Spizek, J. Assay of Tyrosine Hydroxylase Based on High-performance Liquid Chromatography Separation and Quantification of L-Dopa and L-Tyrosine. *Biomed. Chromatogr.* **2007**, *21*, 1252−1258.
(62) Ferreira, P.; Shin, I.; Sosova, I.; Dornevil, K.; Jain, S.; Dewey, D.; Liu, F.; Liu, A. Hypertryptophanemia Due to Tryptophan 2,3-Dioxygenase Deficiency. *Mol. Genet. Metab.* **2017**, *120*, 317−324.
(63) Fielding, A. J.; Dornevil, K.; Ma, L.; Davis, I.; Liu, A. Probing Ligand Exchange in the P450 Enzyme CYP121 from *Mycobacterium tuberculosis*: Dynamic Equilibrium of the Distal Heme Ligand as a Function of pH and Temperature. *J. Am. Chem. Soc.* **2017**, *139*, 17484−17499.

DOI: 10.1021/acscatal.9b00231
ACS Catal. 2019, 9, 4764−4776

Supporting Information

Biocatalytic Carbon-Hydrogen and Carbon-Fluorine Bond Cleavage through Hydroxylation Promoted by a Histidyl-Ligated Heme Enzyme

Yifan Wang[†], Ian Davis[†], Inchul Shin[†], Daniel J. Wherritt[†], Wendell P. Griffith[†], Kednerlin Dornevil[†], Keri L. Colabroy[‡], and Aimin Liu*[,†]

[†]Department of Chemistry, University of Texas, San Antonio, Texas 78249, and
[‡]Department of Chemistry, Muhlenberg College, Allentown, PA 18104, United States

***Correspondence to**:
Aimin Liu, Department of Chemistry, University of Texas at San Antonio, 1 UTSA Circle, San Antonio, TX 78249-0698; Phone: +1-210-458-7062; Fax: 210-458-7428; and E-mail: Feradical@utsa.edu

Table of Contents

Table S1. Thermodynamic analysis of L-tyrosine (**1**), L-phenylalanine (**2**) and *O*-methyl-L-tyrosine (**3**), 3-fluoro-L-tyrosine (**5**), 3-chloro-L-tyrosine (**6**), 3-iodo-L-tyrosine (**7**) binding to LmbB2 as obtained from ITC. The fitting was done for one-site binding model. *N* values for **2** and **3** were adopted from the results of **1**.

Ligand	N	$K_A \times 10^{-3}(M^{-1})$	K_D (μM)	ΔH (kcal/mol)	ΔS (cal/mol/deg)
1	0.24 ± 0.00	739 ± 18	1.35 ± 0.03	-2032 ± 80	-42.5
2	0.24	3.1 ± 0.8	318 ± 8	-7599 ± 98	-9.9
3	0.24	0.77 ± 0.01	1292 ± 22	-1294 ± 141.4	-30.9
5	0.24 ± 0.01	45.1 ± 2.3	22.2 ± 1.1	-1597 ± 493	-33.2
6	0.24	2.9 ± 0.2	346 ± 2	-1916 ± 698	-49.5
7[1]	0.24	0.128 ± 0.003	7817 ± 183	-25650 ± 5110	-865

[1] Values are reported with uncertainty due to weak binding affinity close to the detection limit.

Table S2. Quantitative analysis on products of 3-halogen-L-tyrosines using HPLC. Each substrate reacts with LmbB2 generating two products, i.e., DOPA and 3-halogen-5-hydroxyl-L-tyrosine (3-X-5-OH-Tyr).

Substrate	A_{DOPA}	$A_{3\text{-}X\text{-}5\text{-}OH\text{-}Tyr}$	$A_{unreacted\ substrate}$	$A_{total\ substrate}$	Conversion%	Normalized A_{DOPA}	Relative Ratio
3-Fluoro-L-tyrosine	6.33 ± 0.03	9.83 ± 0.04	27.61 ± 0.24	44.89 ± 0.79	45.2 ± 2.2	14.02 ± 0.70	4.5
3-Chloro-L-tyrosine	2.78 ± 0.15	22.52 ± 0.77	13.94 ± 0.65	43.90 ± 0.53	68.2 ± 3.3	4.07 ± 0.30	1.3
3-Iodo-L-tyrosine	1.28 ± 0.14	12.79 ± 0.75	42.97 ± 2.59	73.15 ± 2.56	41.3 ± 2.9	3.10 ± 0.39	1

Note: Conversion% = $A_{unreacted\ substrate} / A_{total\ substrate}$
Normalized $A_{DOPA} = A_{DOPA}$ / conversion%

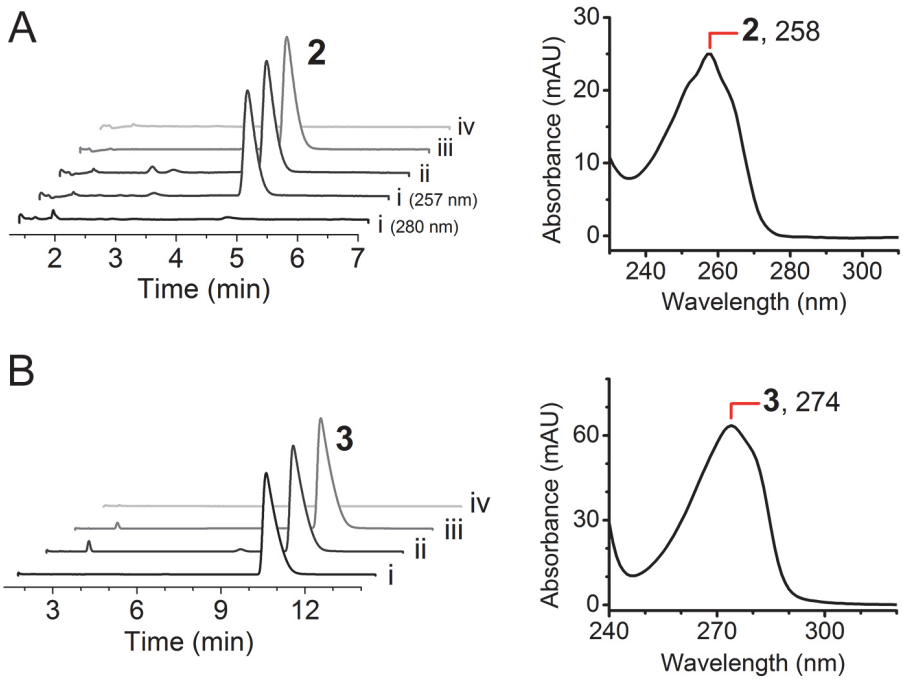

Figure S1. HPLC profile and peak absorbance of LmbB2 reaction with (A) L-phenylalanine (**2**) and (B) *O*-methyl-L-tyrosine (**3**) in the presence of hydrogen peroxide. The enzymatic reaction (i) consisted 100 μM enzyme, 3 mM substrate analog and 3 mM H_2O_2. H_2O_2 was titrated to initiate the reaction by adding multiple times and small volume each time to final concentration of 3 mM to avoid heme bleaching. Three controls consisted (ii) enzyme with substrate analog, (iii) substrate analogue with H_2O_2 and (iv) enzyme with H_2O_2. There was no reaction detected even when up to 20 mM analog concentration was used with both H_2O_2 and PAA. Absorbance was monitored at both 257 and 280 nm for **2** and 280 nm for **3**.

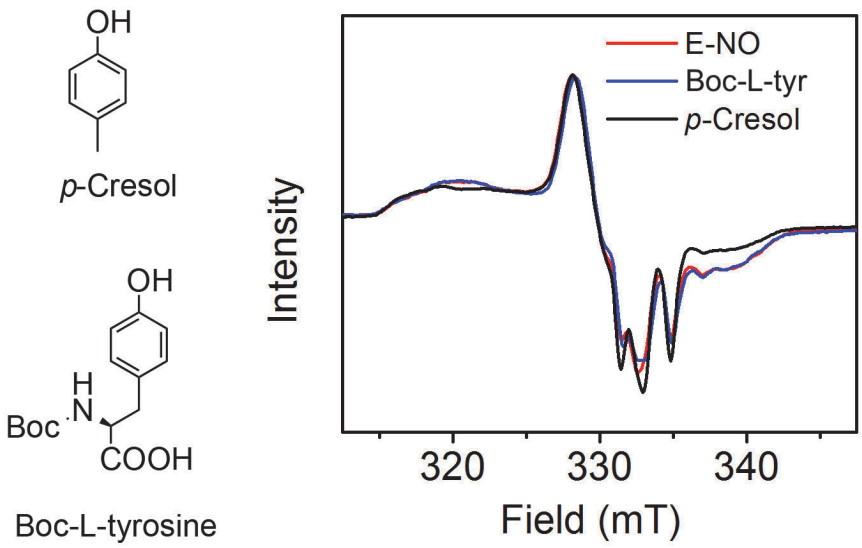

Figure S2. EPR spectra of ferrous enzyme-NO· complex alone and with unbounded phenols, *N*-Boc-L-Tyrosine and *p*-Cresol. The overall EPR signals have no significant difference and g_{ave} values are identical (g_{ave} = 2.030). All spectra were obtained at 50 K, 9.4 GHz microwave frequency and 0.05 mW power.

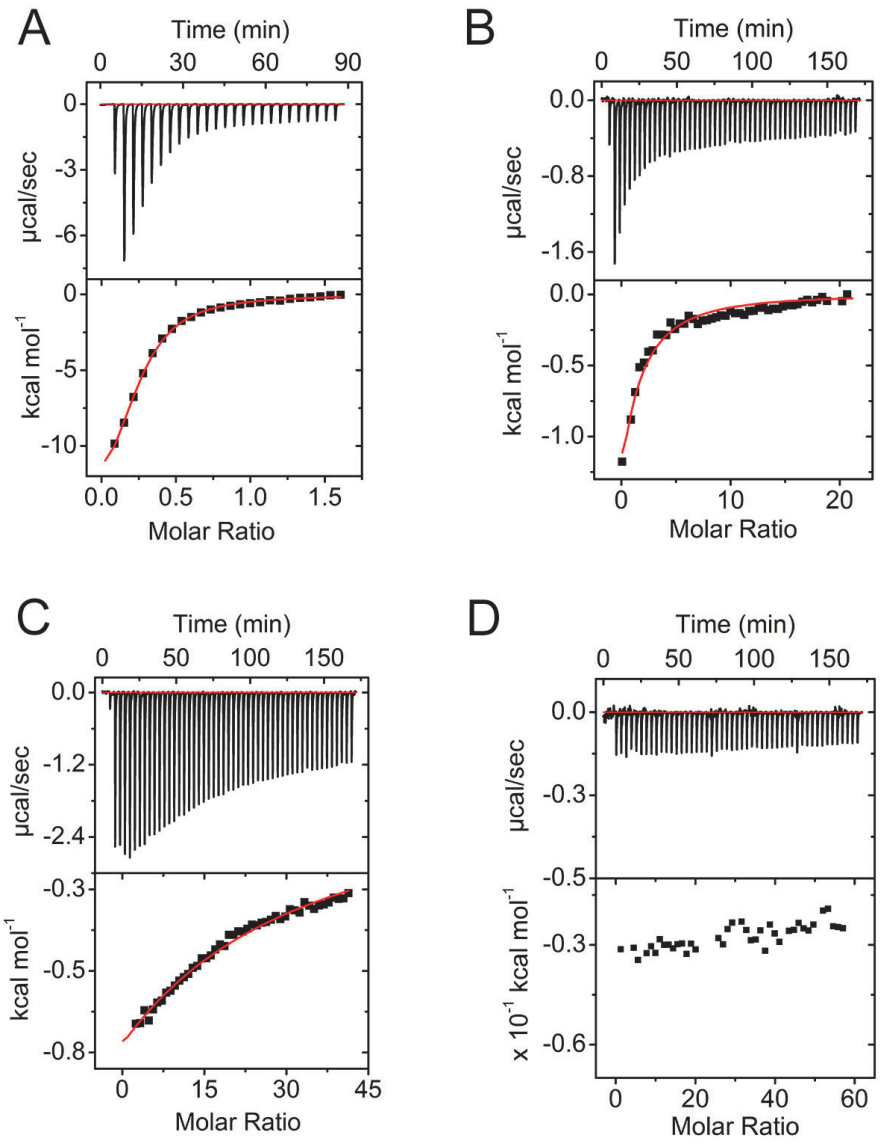

Figure S3. ITC binding assays of LmbB2 with reactive tyrosine analogs. (A) 3-fluoro-L-tyrosine; (B) 3-chloro-L-tyrosine; (C) 3-iodo-L-tyrosine; (D) 3-nitro-L-tyrosine.

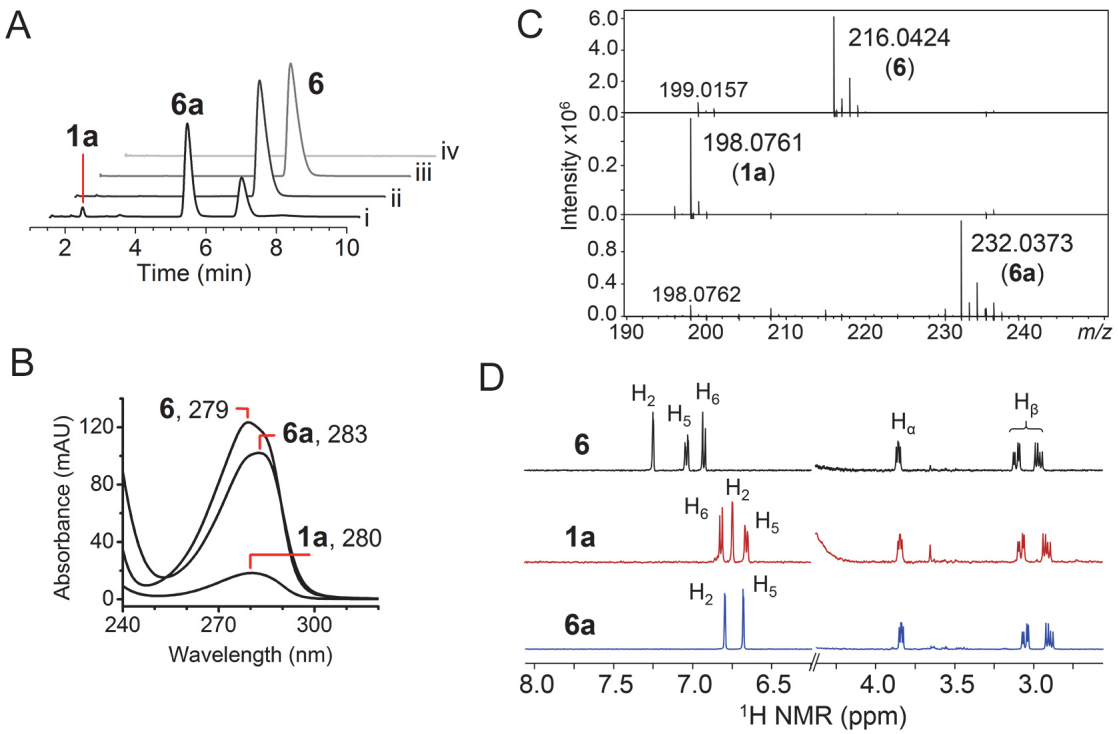

Figure S4. LmbB2 reaction with 3-chloro-L-tyrosine (**6**) generated and L-3,4-dihydroxyphenylalanine (**1a**) and 3-chloro-5-hydroxyl-L-tyrosine (**6a**). (A) Two product peaks were detected by HPLC. The enzymatic reaction (i) consisted 100 μM enzyme, 3 mM **6** and 3 mM H_2O_2. H_2O_2 was titrated to initiate the reaction by adding multiple times and small volume each time to final concentration of 3 mM to avoid heme bleaching. Three controls consisted (ii) enzyme with **6**, (iii) **6** with H_2O_2 and (iv) enzyme with H_2O_2. (B) Absorbance spectra of **6** (blue) and **6a** (black). (C) High-resolution mass spectra of **6**, **1a** and **6a**. (D) ^{1}H NMR analysis **6**, **1a** and **6a**, hydrogen atoms are labeled according to the numbering of carbon.

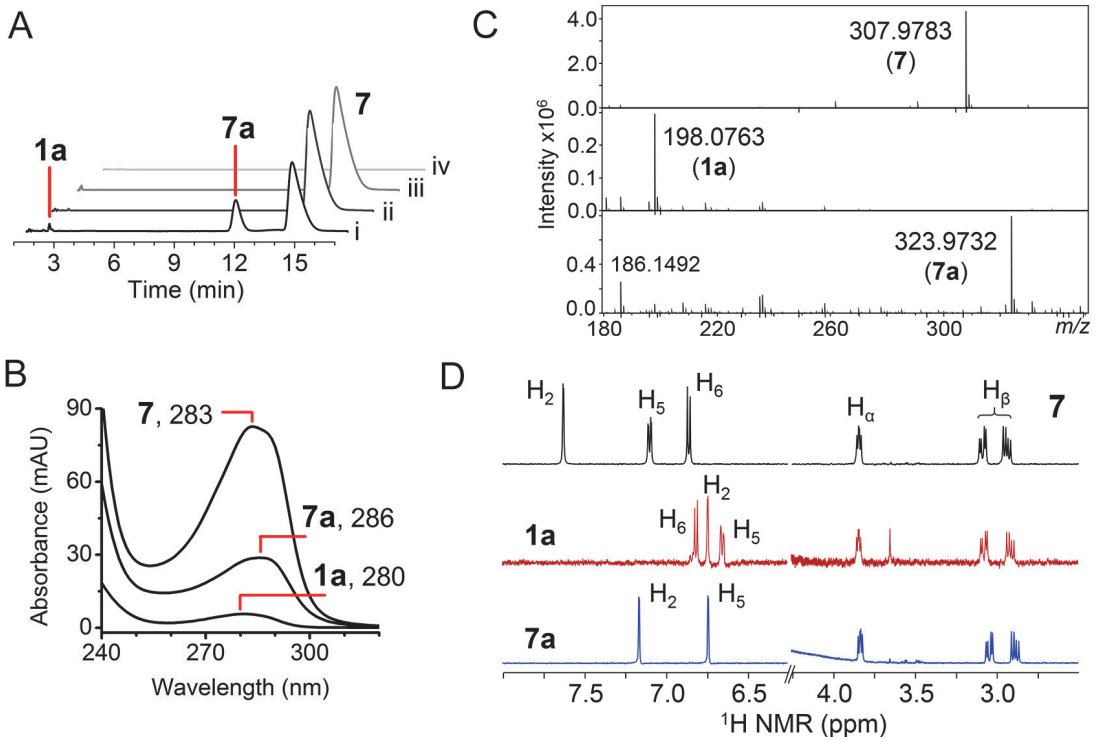

Figure S5. LmbB2 reaction with 3-iodo-L-tyrosine (**7**) generated and L-3,4-dihydroxyphenylalanine (**1a**) and 3-iodo-5-hydroxyl-L-tyrosine (**7a**). (A) Two product peaks were detected by HPLC. The enzymatic reaction (i) consisted 100 μM enzyme, 3 mM **7** and 3 mM H_2O_2. H_2O_2 was titrated to initiate the reaction by adding multiple times and small volume each time to final concentration of 3 mM to avoid heme bleaching. Three controls consisted (ii) enzyme with **6**, (iii) **6** with H_2O_2 and (iv) enzyme with H_2O_2. (B) Absorbance spectra of **6** (blue) and **6a** (black). (C) High-resolution mass spectra of **7**, **1a** and **7a**. (D) ^{1}H NMR analysis **7**, **1a** and **7a**, hydrogen atoms are labeled according to the numbering of carbon.

Kinetic modelling of organic substrates competing with catalase-like activity of LmbB2

Kinetic modelling of the catalase-like activity of LmbB2 competing with increasing organic substrate (L-tyrosine, **1** or 3-fluoro-L-tyrosine, **5**) as described in **Figure 5C** can be approached with a minimal mechanism as shown in **Scheme S1**. In this model, E

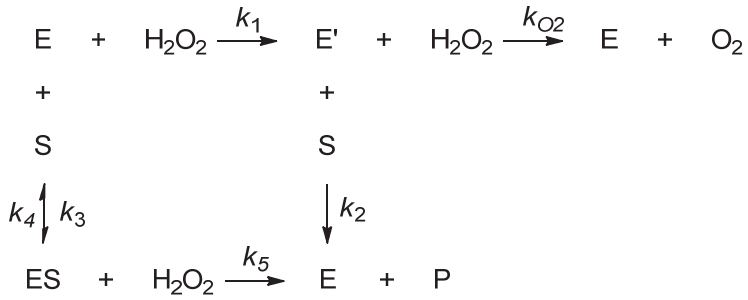

Scheme S1. Minimal competitive model for tyrosine competing with the catalase activity of LmbB2.

represents unbound enzyme, S is the organic substrate, ES is enzyme bound with the organic substrate, E' is the oxidized Compound I-like state of the enzyme, and P is the hydroxylated product, L-3,4-dihydroxyphenylalanine (DOPA, **1a**). Using the Michaelis & Menten framework for deriving steady-state enzyme kinetics, an expression for the rate of O_2 production as a function of S can be determined. The rate of O_2 production is given by eq. 1

$$\frac{d[O_2]}{dt} = k_{O_2} \cdot [E'] \cdot [H_2O_2] \quad (1)$$

As the rate of O_2 production is measureable, and hydrogen peroxide is known, an expression for the concentration of E' must be derived. The differential equation describing the change in concentration of E' is given in eq. 2.

$$\frac{d[E']}{dt} = k_1 \cdot [E] \cdot [H_2O_2] - \left(k_2 \cdot [E'] \cdot [S] + k_{O_2} \cdot [E'] \cdot [H_2O_2]\right) \quad (2)$$

Invoking the steady state assumption, mass balance of the enzyme states where E_T is the total enzyme concentration, and collecting like terms gives [E'] as eq. 3.

$$[E'] = \frac{[E_T] - [ES]}{\left(\frac{k_2 \cdot [S]}{k_1 \cdot [H_2O_2]} + \frac{k_{O_2}}{k_1} + 1\right)} \quad (3)$$

In a similar fashion, an expression for the concentraion of ES can be obtained, eq. 4.

$$\frac{d[ES]}{dt} = k_3 \cdot [E] \cdot [S] - (k_4 \cdot [ES] + k_5 \cdot [ES] \cdot [H_2O_2])$$

$$[ES] = \frac{[E_T] - [E']}{\left(\frac{k_4 + k_5 \cdot [H_2O_2]}{k_3 \cdot [S]} + 1\right)} \quad (4)$$

Substition of ES (eq. 4) into the expression for E' (eq. 3) and subsequently into the initial rate expression for O_2 production (eq. 1) gives the steady-state equation for the initial rate of the production of O_2 by LmbB2 catalase-like activity in competition with the hydroxylation of an organic substrate, eq. 5.

$$V_{0\,O_2} = k_{O_2} \cdot [H_2O_2] \cdot [E_T] \cdot \frac{1 - \frac{1}{D1}}{\left(\frac{k_2 \cdot [S]}{k_1 \cdot [H_2O_2]} + \frac{k_{O_2}}{k_1} + 1 - \frac{1}{D1}\right)} \quad (5)$$

$$D1 = \left(\frac{k_4 + k_5 \cdot [H_2O_2]}{k_3 \cdot [S]} + 1\right)$$

The trend of the data obtained from competing LmbB2 catalase-like activity with its native substrate, **1**, is well captured by eq. 5, however data obtained using the alternate substrate, **5**, does not aproach zero at high substrate concentrations and is not well described by above 100 μM, **Figure S6**.

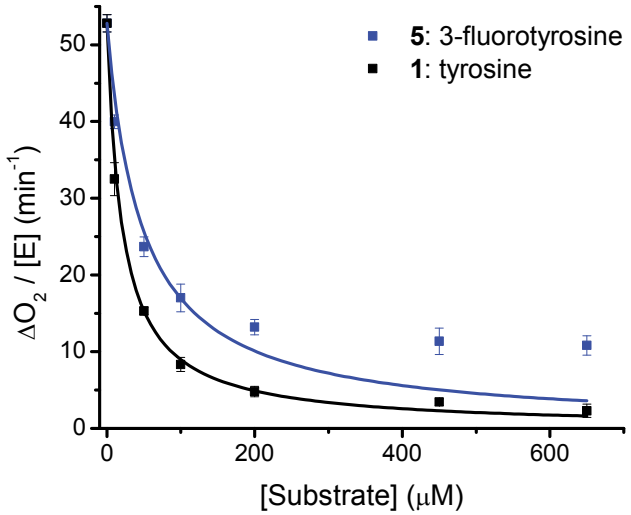

Figure S6. Catalase competition assays as fit by Scheme S1.

If a portion of **5** reacts with LmbB2 and hydrogen peroxide as described in **Figure 8** to generate DOPA and oxidized LmbB2, then another equivalent of hydrogen peroxide would be required to return LmbB2 to its resting state for the next round of reactions. As such, the competition mechanism of **5** should be distinct from **1**, as it requires that the enzyme may be left in an oxidized state after reaction, **Scheme S2**.

Similar as was done above, **Scheme S2** can be used to generate an expression for the rate of O_2 production as a function of a substrate which can react normally (k_5) to produce P1 or produce P2 (DOPA in the case of fluorotyrosine) via k_6 while leaving the enzyme in an oxidized state, E', which then requires hydrogen peroxide to return to the resting state. The differential equation which describes the change in concentration of E' is given by eq. 6.

$$\frac{d[E']}{dt} = k_1 \cdot [E] \cdot [H_2O_2] + k_6 \cdot [ES] \cdot [H_2O_2] - \left(k_2 \cdot [E'] \cdot [S] + k_{O_2} \cdot [E'] \cdot [H_2O_2]\right) \quad (6)$$

Invoking the steady state assumption, mass balance, and collecting like terms gives [E'] as eq. 7.

$$[E'] = \frac{k_1 \cdot [E_T] + [ES] \cdot (k_6 - k_1)}{\left(\frac{k_2 \cdot [S]}{[H_2O_2]} + k_{O_2} + k_1\right)} \quad (7)$$

In a similar fashion, an expression for the concentraion of ES can be obtained, eq. 8.

$$\frac{d[ES]}{dt} = k_3 \cdot [E] \cdot [S] - [ES] \cdot (k_4 + k_5 \cdot [H_2O_2] + k_6 \cdot [H_2O_2])$$

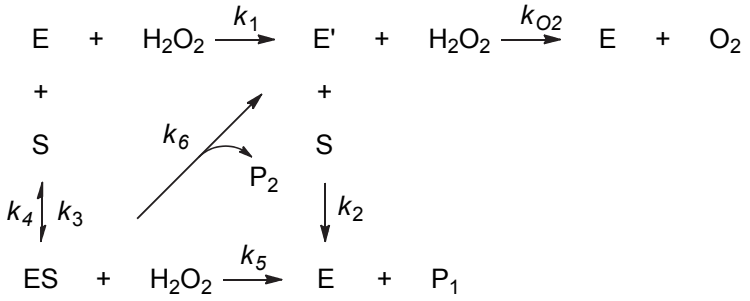

Scheme S2. Minimal competitive model for 3-fluorotyrosine competing with the catalase activity of LmbB2.

$$[ES] = \frac{[E_T] - [E']}{\left(\frac{k_4 + (k_5 + k_6) \cdot [H_2O_2]}{k_3 \cdot [S]} + 1\right)} \quad (8)$$

Substition of ES (eq. 8) into the expression for E' (eq. 7) and subsequently into the initial rate expression for O_2 production (eq. 1) gives the steady-state equation for the initial rate of the production of O_2 by LmbB2 catalase activity in competition with the hydroxylation of an organic substrate which can also undergo nucleophilic aromatic substitution, leaving the enzyme in an oxidized state, eq. 9.

$$V_{0\,O_2} = k_{O_2} \cdot [H_2O_2] \cdot [E_T] \cdot \frac{k_1 + \frac{k_6 - k_1}{D2}}{\left(\frac{k_2 \cdot [S]}{[H_2O_2]} + k_{O_2} + k_1 + \frac{k_6 - k_1}{D2}\right)} \quad (9)$$

$$D2 = \left(\frac{k_4 + (k_5 + k_6) \cdot [H_2O_2]}{k_3 \cdot [S]} + 1\right)$$

As shown in **Figure S7**, inclusion of a pathway by which **5** may react with LmbB2 and peroxide leaving the enzyme in an oxidized state which must react with hydrogen peroxide, producing O_2, to return to the resting state produces an equation which captures the observed behavior. Fitting the data of catalase activity being inhibited by **5** requires ca. 24% of the reaction to proceed via the nucleophilic aromatic substitution reaction pathway that produces DOPA and oxidized enzyme. The equation derived from **Scheme S2** can also provide satisfactory description of the tyrosine reaction if the k_6 parameter is set to zero. In all cases, k_{O2} and k_1 are constrained to the minimal values that produce the correct activity when no organic substrate is present. Similarly, the k_5 value is set at the k_{cat} for this activity of 34 min^{-1}. The other microscopic rate constants are not well bounded, so this kinetic analysis should be considered descriptive rather than quantiative. Both eq. 5 and eq 9 were able to fit the experimental data with either k_2 or k_3 as a large number with the other near zero; fittings with intermediate values produced sigmodial lineshapes which do not describe the data. However, fitting with a large k_2 and near zero k_3 does not make physical sense, as the K_d for substrate binding is known to be in the micromolar range, therefore this analysis demonstrates that organic substrates are not kinetically competent to compete with hydrogen peroxide for a preformed oxidized enzyme.

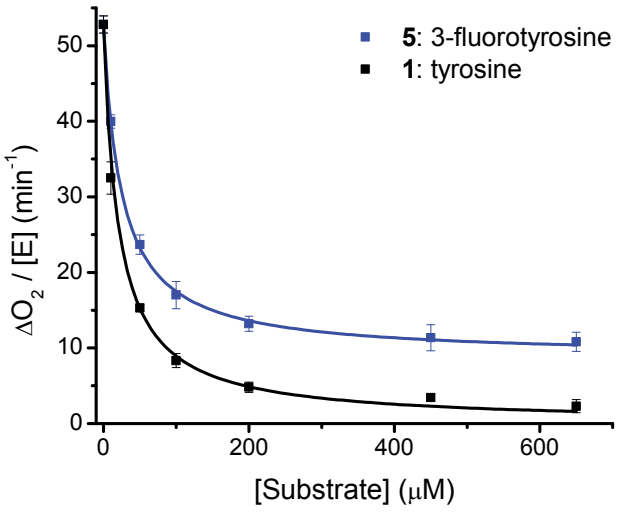

Figure S7. Catalase competition assays as fit by Scheme S2.

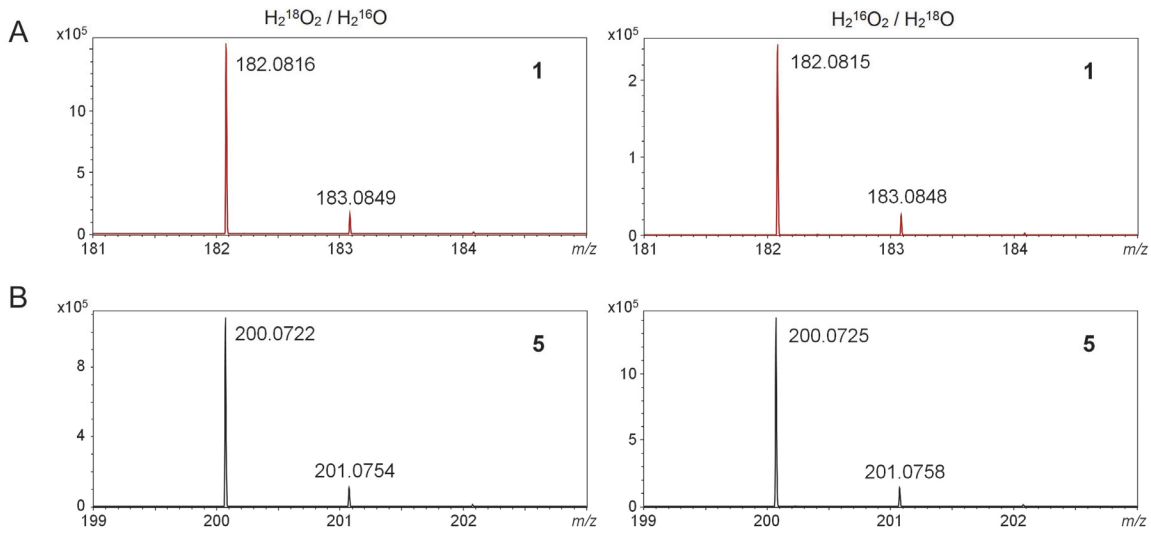

Figure S8. MS analyses on unreacted substrates with ^{18}O labeled H_2O and H_2O_2. L-tyrosine (**1**) (A) and 3-fluoro-L-tyrosine (**5**) (B)were used as substrates. Reactions were carried out with isotope labeled water (left) or hydrogen peroxide (right).

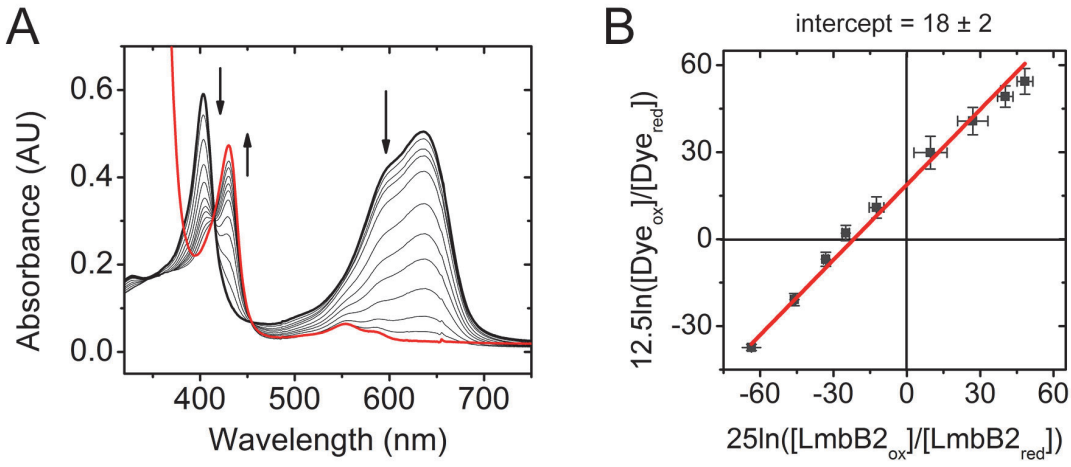

Figure S9. LmbB2 redox potential measurement. (A) Representative spectra for the reduction of LmbB2 and Nile Blue. (B) Corresponding Nernst plot with 3 repeated trials. Linear fitting (red line) yielded a y-intercept of 18 ± 2.

NMR data for tyrosine analogs and their products

Peak assignments were based on coupling constant and chemical shift.

1a, ^{1}H NMR (500 MHz, D_2O) δ 6.87 (d, *J* = 8.1 Hz, 1H), 6.80 (d, *J* = 1.9 Hz, 1H), 6.71 (dd, *J* = 8.3, 1.8 Hz, 1H), 3.90 (dd, *J* = 7.9, 5.0 Hz, 1H), 3.13 (dd, *J* = 14.7, 5.1 Hz, 1H), 2.97 (dd, *J* = 14.7, 7.9 Hz, 1H).

4, ^{1}H NMR (500 MHz, D_2O) δ 7.97 (d, *J* = 2.2 Hz, 1H), 7.50 (dd, *J* = 8.6, 2.3 Hz, 1H), 7.11 (d, *J* = 8.6 Hz, 1H), 3.91 (dd, *J* = 7.2, 5.8 Hz, 1H), 3.18 (dd, *J* = 14.7, 5.6 Hz, 1H), 3.09 (dd, *J* = 14.7, 7.4 Hz, 1H).

4a, ^{1}H NMR (500 MHz, D_2O) δ 7.57 (s, 1H), 7.13 (s, 1H), 3.94 (dd, *J* = 7.4, 5.6 Hz, 1H), 3.18 (dd, *J* = 14.8, 5.4 Hz, 1H), 3.06 (dd, *J* = 14.7, 7.6 Hz, 1H).

5, ^{1}H NMR (500 MHz, D_2O) δ 7.00 (d, *J* = 12.2 Hz, 1H), 6.96 – 6.86 (m, 2H), 3.86 (dd, *J* = 7.9, 5.2 Hz, 1H), 3.11 (dd, *J* = 14.7, 5.2 Hz, 1H), 2.97 (dd, *J* = 14.7, 7.8 Hz, 1H). ^{19}F NMR (471 MHz, D_2O) δ -137.68 (dd, *J* = 12.5, 9.2 Hz).

5a, ^{1}H NMR (500 MHz, D_2O) δ 6.59 (dd, *J* = 11.0, 2.1 Hz, 1H), 6.56 (d, *J* = 2.0 Hz, 1H), 3.85 (dd, *J* = 7.9, 5.1 Hz, 1H), 3.06 (dd, *J* = 14.7, 5.0 Hz, 1H), 2.91 (dd, *J* = 14.7, 7.9 Hz, 1H). ^{19}F NMR (471 MHz, D_2O) δ -137.58 (d, *J* = 10.0 Hz).

6, ^{1}H NMR (500 MHz, D_2O) δ 7.25 (d, *J* = 1.8 Hz, 1H), 7.03 (dd, *J* = 8.4, 1.9 Hz, 1H), 6.92 (d, *J* = 8.4 Hz, 1H), 3.85 (dd, *J* = 7.8, 5.3 Hz, 1H), 3.11 (dd, *J* = 14.7, 5.3 Hz, 1H), 2.96 (dd, *J* = 14.7, 7.8 Hz, 1H).

6a, ^{1}H NMR (500 MHz, D_2O) δ 6.80 (d, *J* = 1.9 Hz, 1H), 6.68 (d, *J* = 1.9 Hz, 1H), 3.84 (dd, *J* = 7.9, 5.1 Hz, 1H), 3.05 (dd, *J* = 14.7, 5.1 Hz, 1H), 2.90 (dd, *J* = 14.7, 7.9 Hz, 1H).
7, ^{1}H NMR (500 MHz, D_2O) δ 7.63 (d, *J* = 2.0 Hz, 1H), 7.10 (dd, *J* = 8.3, 2.0 Hz, 1H), 6.86 (d, *J* = 8.2 Hz, 1H), 3.90 – 3.76 (dd, *J* = 7.8, 5.1 Hz, 1H), 3.09 (dd, *J* = 14.7, 5.2 Hz, 1H), 2.94 (dd, *J* = 14.8, 7.8 Hz, 1H).

7a, ^{1}H NMR (500 MHz, D_2O) δ 7.16 (d, *J* = 1.8 Hz, 1H), 6.74 (d, *J* = 1.8 Hz, 1H), 3.83 (dd, *J* = 7.8, 5.1 Hz, 1H), 3.04 (dd, *J* = 14.7, 5.1 Hz, 1H), 2.89 (dd, *J* = 14.7, 7.9 Hz, 1H).